School of Chemistry

FUNCTIONALISED DIAMOND SURFACES USING A TUBE FURNACE

Mulang Shu

This thesis is submitted in partial fulfilment of the requirements for the Honours Degree of MSci at the University of Bristol

Supervisor: Professor Paul May

Second Assessor: Professor David Fermin

Physical and Theoretical Chemistry

Contents

Statement of Limiting Factors

The progress of this project was significantly impacted by a series of factors beyond my control:

1. Delays were initially encountered due to the time required to obtain safety approval for laboratory access, as limited information was provided regarding this process. This resulted in a postponed commencement of experimental work.
2. Access to laboratory facilities was subsequently restricted due to a three-week closure for air conditioning maintenance. Furthermore, upon reopening, essential apparatus, the tube furnace remained unavailable until maintenance was completed, resulting in additional delays to planned experimental procedures.
3. Time had been allocated during the Christmas preparation period to mitigate earlier delays; however, an unforeseen incident involving a laboratory extraction fan fire led to a further shutdown of facilities for approximately two to three weeks, preventing the continuation of experimental work.
4. Communication delays and limited responsiveness from external analytical services constrained the timeframe available for data acquisition, subsequent analysis, and further optimisation of experimental conditions.

Collectively, these factors resulted in a substantial compression of the experimental timeline, limiting the scope of work that could be undertaken and reducing the extent of data collection and analysis achievable within the project period. Nevertheless, efforts were made to adapt the project plan and maximise the reliability and quality of the results obtained within the available constraints.

Acknowledgements

I would like to express my sincere gratitude to my supervisor, Professor Paul May, for his guidance, support, and patience throughout this project, particularly during challenging times. I am also grateful to the Bristol University Diamond Group (BUDGies) for making my final year at university such a wholesome and enjoyable experience. Their warmth and welcoming nature made a lasting impact on me.

This thesis represents the final piece of work in my MSci degree, a journey that coincided with one of the most difficult periods of my life, both academically and personally. It has not been an easy path, and I am truly grateful to my family and friends for their constant support.

I am especially grateful to my mother, Juan Zhang, for giving me the opportunity to study at this institution and for her encouragement and strength throughout.

I would also like to acknowledge my grandmothers, Shuqin Fan and Shuhua Fan, who have been my anchors throughout my life. Their support and love have kept me grounded, and it is because of them that I have been able to pursue my studies.

My sincere thanks go to Geraldine Ozor, Rebecca Coffey, and Jemima Kellett, who treated me like their own daughter in a foreign country, for their kindness, care, and support during this journey. Their care, particularly during difficult times, has meant more to me than words can express.

I am also grateful to Áine Davis for her constant faith in me and her reassurance; Huiwen Ouyang for being there for me with her wise counsel; Sam Leon for his constant support and encouragement despite my procrastination; and Ellen Young for her steadfast support during some of my most challenging moments.

I extend my heartfelt thanks to all my friends who have supported and cared for me throughout the years. Their presence has been invaluable, and I feel incredibly fortunate to have them in my life.

Finally, I dedicate this thesis to my father, Guofeng Shu; my grandfathers, Jingxiang Shu and Hongbin Zhang; my uncle, Guoyao Shu; and my grandmother, Yuqing Li. Though they are no longer here, I know they would be proud of this moment. This work is in loving memory of them.

Symbols and Acronyms

Φ	Work Function
eV	Electron Volts
χ	Electron Affinity
E_{vac}	Vacuum Level
E_{CBM}	Conduction Band Minimum
hν	UV Excitation Energy
E_{VBM}	Valence Band Minimum
EF	Fermi Level
J	Emission Current Density
AR	Richardson Constant
k	Boltzmann Constant
T	Absolute Temperature
η(Carnot)	Carnot Efficiency
EG	Band Gap
°C	Degrees Celsius
Å	Ångströms
sccm	Standard Cubic Centimetres per Minute
VBM	Valence Band Maximum
CVD	Chemical Vapour Deposition
SCD	Single Crystal Diamond
NEA	Negative Electron Affinity
PEA	Positive Electron Affinity
SEM	Scanning Electron Microscopy
CBM	Conduction Band Minimum
VBM	Valence Band Maximum
MWCVD	Microwave-plasma Chemical Vapour Deposition
HFCVD	Hot Filament Chemical Vapour Deposition
MW	Microwave Power
FTIR	Fourier Transform Infrared (FTIR) Spectroscopy
CB	Conduction Band
VB	Valence Band
TEC	Thermionic Energy Converter
UHV	Ultra-high Vacuum
UPS	Ultraviolet Photoelectron Spectroscopy
KE	Kinetic Energy
BE	Binding Energy
XPS	X-ray Photoelectron Spectroscopy
PEEM	Photoemission Electron Microscopy
HPHT	High Pressure High Temperature

Abstract

Diamond has attracted significant interest for thermionic emission applications owing to its excellent thermal stability, wide band gap (~5.4 eV), and ability to exhibit negative electron affinity (NEA) after surface termination. Hydroxyl (OH) termination has recently been proposed as a promising method to achieving low work function, thermally robust NEA diamond surfaces that could be utilised in thermionic energy converters. This project aimed to investigate whether a complete OH termination could be achieved on single crystal CVD (100) diamond via high-temperature water vapour annealing process.

A tube furnace was commissioned and used to treat pre-hydrogen-terminated diamond samples under moist nitrogen flow at temperatures ranging from 500 °C to 900 °C. The resulting surfaces were characterised using FTIR, XPS, and UPS to assess their chemical composition and electronic properties.

XPS confirmed that all samples retained predominantly sp^3 hybridised carbon, indicating preservation of the diamond structure post treatment, while also revealing oxygen-containing species consistent with C–O and C–OH environments. A clear temperature dependence was observed, with lower temperatures favouring oxygen retention and higher temperatures promoting its removal. Unfortunately, it was not possible to conclusively confirm full hydroxyl termination. However, complete hydroxyl termination could not be confirmed. FTIR did not show clear C-OH features, overlapping species within XPS spectra limited definitive assignment, and UPS was affected by sample charging, thus, preventing reliable determination of work function and electron affinity.

Overall, while water vapour annealing modified the diamond surface and introduced oxygen-based functionalities, but complete and well-defined OH termination was not achieved. These findings highlight the sensitivity of diamond surface chemistry to processing conditions and the need for improved control and characterisation before employing it in thermionic emission applications.

1.1 Structure and Properties of Diamond

Diamonds are the hardest naturally occurring materials, a property that arises from their strong covalent sp^3 bonds. They exhibit an extremely high Young's modulus, exceeding 1000 GPa, can withstand compressive stresses of at least 60 GPa,[1] and are among the least compressible materials known. In addition, diamond has the highest thermal conductivity at room temperature and is both chemically and biologically inert.[2]

The natural formation of diamond occurs over approximately one billion years, deep within the Earth's mantle, under conditions of extremely high pressure and temperature.[3] Under these extreme conditions, carbon atoms arrange into a "metastable" carbon allotrope with a face-centred cubic (FCC) structure. The diamond lattice can be described as two interpenetrating FCC lattices displaced along the body diagonal by (¼, ¼, ¼), with two carbon atoms per primitive (Bravais) cell. The unit cell of diamond consists of eight corner atoms, six face-centred atoms, and four atoms located along the cube diagonals, as shown in Figure X. The diamond lattice has a lattice constant of 3.57 Å and a carbon–carbon bond length of 1.54 Å.[4]

Due to its tetrahedral structure, each carbon atom forms sp^3 hybridised covalent bonds with four neighbouring carbon atoms, as shown in Figure 1. As a result of this rigid, fully three-dimensional lattice structure, diamond contains no interlayer spacing. Despite the relatively long carbon–carbon bond length, this efficient packing leads to an exceptionally high atomic density of 1.76×10^{23} cm^{-3}, the highest of any known solid.[5]

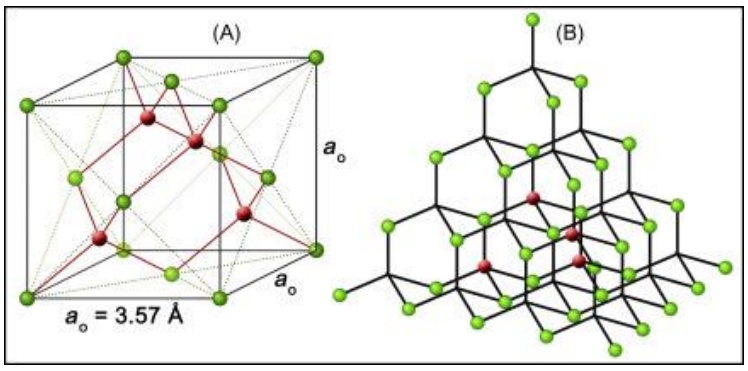

Figure 1 (A) Schematic chemical structure of a unit cell of diamond crystal and (B) tetrahedral structure of diamond, each atom forming bonds with its four nearest neighbours.[4]

The extended timescale and extreme conditions required for diamond formation have led to the rarity of diamond in nature. Although the diamond trade can be traced back to India approximately 2500 years ago, diamonds were largely limited to use as jewellery for the elite owing to their rarity and high value.[6]

It was not until the development of the high-pressure, high-temperature (HPHT) diamond synthesis technique in the 1950s that diamonds began to see broader applications.[7]

1.2 High Pressure, High Temperature Diamond

High-pressure, high-temperature (HPHT) synthesis is the earliest industrial route for producing diamond in large quantities, with sizes ranging from nanometres to millimetres. A key feature of HPHT synthesis is the use of catalyst systems to reduce the energy barrier for the graphite-to-diamond transition. To this day, this technique remains a cornerstone of lab-grown diamond manufacturing. This method replicates the thermodynamic conditions under which natural diamond forms in the Earth's mantle, typically exceeding 5 GPa and 1700 K, allowing the transformation of carbon sources such as graphite into diamond.[8]

There are three fundamental approaches in HPHT synthesis: the solubility gradient method, the temperature gradient growth method, and the direct transformation method.

The solubility gradient method enables controlled epitaxial diamond growth, although the achievable crystal size is often limited to no more than 1 mm. In this method, the carbon source is dissolved into a molten transition metal catalyst such as iron, nickel or cobalt, which tends to lower the pressure and temperature required for the graphite-to-diamond transition. Carbon then diffuses through the melt and precipitates onto a seed crystal, driven by differences in carbon solubility between graphite and diamond stability regions. The presence of a metallic solvent is essential in this method.

The temperature gradient growth (TGG) method operates near thermodynamic equilibrium, producing diamond crystals of very high quality. It is the most effective method for the synthesis of large, high-quality single-crystal diamond (SCD). Within the process, a metallic flux containing dissolved carbon sources is subjected to pressures of approximately 5–5.5 GPa and temperatures of 1350–1450 °C. A temperature gradient is then applied, which drives diamond growth on a seed crystal.[8]

In contrast, the direct transformation method allows graphite-to-diamond conversion without the presence of a solvent catalyst. This method is typically used in the formation of polycrystalline diamonds rather than SCD. The process usually requires much higher pressures and temperatures, typically over 13 GPa and 1300 K respectively, thus bypassing the intermediate molten phases.[9]

In comparison to the time consuming natural diamond growth in the Earth's mantle, a primary advantage of HPHT synthesis is that it is able to produce large, high-purity SCD within several days to weeks. This allows HPHT diamonds to be incorporated into demanding industrial applications such as cutting and polishing tools, as well as in abrasive applications, where mechanical robustness and wear resistance are critical. Nevertheless, in recent years, advancements in HPHT diamond growth have also enabled the production of gemstone-quality diamonds, expanding the commercial importance of this technique.[2]

However, the extreme pressure and high operational temperature conditions associated with HPHT diamond synthesis result in high operational costs and safety concerns. The growth process of HPHT diamonds also introduces high residual stresses within the crystal lattice,[10] and the resulting crystallographic defects may compromise the material's performance.

The above factors are particularly challenging in applications requiring ultra-high precision, as these structural imperfections can lead to degradation of cutting efficiency and surface finish.[2]

While HPHT remains highly effective for bulk crystal production and industrial tooling, this method offers limited flexibility in controlling complex geometries, restricting its applicability in advanced device fabrication.[2] There has been a growing shift towards alternative diamond synthesis techniques, such as chemical vapour deposition (CVD). CVD offers more control over microstructure and material uniformity, making it more suitable for applications requiring precision and tailored properties.[11]

1.3 Chemical Vapour Deposition of Diamond

In 1960, J. M. Blocher proposed that Chemical vapour deposition (CVD) is a key technique for producing diamond thin films through atom-by-atom growth on a substrate.[12] CVD diamond is widely utilised in the fabrication of diamond-coated tools, enabling the deposition of high-purity diamond films onto complex geometries. The resulting coatings exhibit properties comparable to natural diamond and can be tailored to specific machining requirements and applications. However, weak adhesion between the diamond film and substrate remains a significant limitation, often leading to delamination during operation and reducing tool lifespan and machining quality. Despite this, CVD diamond remains highly promising for industrial and high-technology applications.[2]

CVD growth involves the activation of gaseous precursors in a low-pressure environment (typically 10 - 200 Torr), followed by deposition onto a heated substrate (800 - 1000 °C). Methane diluted in hydrogen is commonly used as the carbon source, with hydrogen playing a critical role in stabilising the growing diamond surface and removing non-diamond carbon.[13] High-quality films are typically achieved at low carbon concentrations, using approximately 1% CH_4, while small additions of oxygen can enhance growth rate and crystallinity.[14]

The compatibility in lattice structure and thermal expansion is required to minimise stress and prevent delamination, making substrate selection crucial. Common substrates include silicon, tungsten-based materials, and diamond itself. The nature of the substrate, together with growth conditions, determines whether the resulting material is single-crystal or polycrystalline diamond.

Several CVD methods are employed, including hot filament CVD (HFCVD),[15] microwave plasma CVD (MWCVD),[16] and DC arc jet plasma techniques.[17] HFCVD is a relatively simple and cost-effective method for producing polycrystalline diamond films.[15] MWCVD offers improved control and higher growth rates, often exceeding 10 $\mu m\ h^{-1}$.[16] In contrast, DC arc jet methods can achieve very high growth rates but typically result in lower-quality material. A major advantage of CVD is the ability to control material properties and introduce dopants. However, poorly optimised conditions may lead to nanocrystalline films with increased sp^2 carbon content, which can reduce diamond-like properties but may enhance electrical conductivity.[18]

Following deposition, the crystallographic orientation of diamond significantly influences film morphology and properties. Growth occurs predominantly on the (100) and (111) planes, which exhibit square and triangular surface geometries, respectively.[16] The relative growth rates of these orientations depend on deposition conditions and are described by the α parameter, as shown in Equation 1,[19] where $\boldsymbol{v_{100}}$ and $\boldsymbol{v_{111}}$ are the growth velocities in each direction. This parameter governs crystal shape, with lower values favouring (100) dominated cubic structures and higher values favouring (111) dominated octahedral morphologies. While in

polycrystalline films, this parameter determines whether square or triangular faceting predominates.[16]

Equation 1

$$\alpha = \sqrt{3}\frac{v_{100}}{v_{111}}$$

These orientation-dependent growth rates arise from the underlying CVD growth mechanism. Since the atomic arrangement differs between (100) and (111) planes, the growth kinetics on each surface differs as the availability and reactivity of surface sites vary. Thus, small changes in growth conditions can significantly alter the balance between (100) and (111) growth, producing films that range from randomly oriented to highly textured structures. While control over the (100) / **(**111) growth ratio enables tailoring of film morphology, this dependence on growth conditions highlights the challenge of achieving consistent orientation. Consequently, precise control of deposition parameters remains essential for optimising film quality and performance in advanced applications.[16]

1.4 Electron emission

Electron emission refers to the physical phenomenon in which external stimulation causes electrons to be ejected from a solid surface. To be emitted from the surface, electrons must acquire sufficient energy to overcome the material's work function, ϕ, which represents the potential energy barrier situated at the surface-vacuum interface, defined as the energy difference between the Fermi level and vacuum level. Once electrons gain enough energy to surpass this barrier, they can subsequently escape into vacuum.[20]

Field emission, photoelectric emission, secondary emission, and thermionic emission are the four primary mechanisms by which electron emission occurs.[21]

Field emission, also known as cold-cathode or auto-electronic emission, does not rely on thermal energy and can therefore occur at relatively low temperatures, including room temperature.[22] This mechanism occurs when a sufficiently strong positive electric field, typically on the order of several megavolts per centimetre, is applied near the surface of a conductive material. This electric field exerts a strong attractive force on the electrons, enabling them to overcome the potential barrier and escape from the material into vacuum.[21]

Photoelectric emission occurs when a beam of light strikes the surface of a material, and electrons absorb the photon energy. If the photon energy exceeds the material's work function, the electrons will gain sufficient energy to escape into vacuum. The emitted electrons are known as photoelectrons, and thus, the process is referred to as the photoelectric effect. The quantity of electron emission is proportional to the light intensity striking the material, provided the photon energy is sufficient to allow the electrons to overcome the work function.[21]

Secondary electron emission occurs when the material surface is bombarded with incoming high-speed particles, such as electrons or ions, collectively referred to as primary particles. The kinetic energy from these incident particles is transferred to the free electrons within the material; those that are subsequently emitted are known as secondary electrons. Once the electrons accumulate sufficient energy, they can overcome the attractive potential of the nuclei and escape from the surface. The quantity of secondary electron emission is dependent on the energy and flux of the primary particles, as well as the properties of the material.[21] However, secondary emission can be undesirable in some electronic devices, causing effects such as negative resistance, while in other applications it is deliberately exploited, for example in electron multipliers and cathode ray tubes.[23]

Thermionic emission occurs as a result of thermal excitation. Upon heating a material, thermal energy is converted into kinetic energy, allowing electrons to gain sufficient energy to overcome the work function and escape into vacuum.[20] The emission is strongly temperature dependent, with the number of emitted electrons increasing rapidly with temperature. Materials with lower work functions require far less thermal energy for electron emission and can therefore operate at much lower temperatures. For example, pure tungsten typically requires temperatures of around 2300 °C, whereas oxide-coated emitters, such as barium or strontium oxides, can achieve emission at temperatures as low as 750 °C. Due to the need to prevent scattering of emitted electrons, thermionic emission is typically carried out under vacuum conditions.[21]

Electron emission is the fundamental basis for modern technologies such as emissive flat-panel displays, spacecraft ion engines, high-power microwave amplifiers, X-ray sources, electron microscopy, and electron-beam lithography techniques.[24–28]

Among the mechanisms mentioned above, thermionic emission, where electrons are emitted due to thermal excitation at increased temperatures, is crucial in high-temperature electron-emitting systems and forms the primary focus of this study.

The Pauli exclusion principle states that each energy state can be occupied by a maximum of two electrons with opposing spins. Electrons therefore fill lower energy states before higher ones.[29] In semiconductors at typical operating temperatures, the valence band, which is a lower-energy band, is usually fully or partially occupied, while the conduction band, a higher-energy band, remains largely unoccupied. These bands are separated by an energy band gap, typically on the order of a few electronvolts (e.g. ~1.1 eV for silicon and ~5.5 eV for diamond), which determines how readily electrons can be excited into the conduction band.[30] Consequently, the energy required for electron emission, characterised by the work function, is also typically several electronvolts.[20]

As a result, substantial energy input is required to enable electrons to overcome the energy barrier and to be emitted into vacuum. This can be achieved either via ultraviolet photon excitation or through thermal activation at temperatures above 1500 K.[20]

1.5 Negative Electron Affinity

Electron affinity, χ, is defined as the energy difference between the conduction band minimum and the vacuum level, representing the barrier that inhibits electrons in the conduction band from escaping into the vacuum.[31]

In certain materials, the conduction band minimum lies above the vacuum level, a condition known as negative electron affinity (NEA), which facilitates electron emission.[20,32] As a result, electrons in the conduction band can escape directly into the vacuum without overcoming an emission barrier. Consequently, electrons initially residing in the valence band only require sufficient energy to be excited into the conduction band, after which emission takes place spontaneously, substantially lowering the overall energy requirement.[20]

Alternatively, the conduction band minimum may lie below the vacuum level; in this case, the material exhibits positive electron affinity (PEA).[33] Electrons excited from the valence band into the conduction band must acquire additional energy to overcome the emission barrier before escaping into vacuum, resulting in less efficient electron emission compared to NEA systems.[20,33]

1.6 Thermionic Emission

Thermionic emission is the process by which electrons are emitted from a material surface as a result of thermal excitation, typically under vacuum. As the temperature increases, electrons gain sufficient thermal energy to overcome the work function, ϕ, and escape into vacuum. This process was first proposed by Owen Willans Richardson in 1901 and later formalised by Saul Dushman in 1930 in the Richardson–Dushman equation:[34,35]

Equation 2

$$J(T) = A_R T^2 \exp\left(\frac{\phi}{kT}\right)$$

Where J is the emission current density, T is the absolute temperature, ϕ is the work function, k is the Boltzmann constant, and A_R is the Richardson constant,[36,37] given by:

Equation 3

$$A_R = \frac{4\pi m k^2 e}{h^3} = 120.2\ A\ cm^{-2}\ K^{-2}$$

Here, m and e denote electron mass and charge, respectively, and h represents Planck's constant.

The emission current density, J, is strongly dependent on the work function and, to a lesser extent, temperature. As the work function increases, a higher temperature is required to achieve electron emission, and vice versa.

For conventional materials exhibiting positive electron affinity (PEA), with work functions typically in the range of 3 - 5 eV, very high operating temperatures, often exceeding 1500 K,[38,39] are required to achieve practical emission current densities greater than 1 A cm^{-2}.

However, heating to such high temperatures is particularly challenging, owing to material degradation and high energy consumption, which limits the practical implementation of thermionic devices.

In contrast, materials exhibiting negative electron affinity (NEA), such as diamond, offer a significant advantage. Due to the absence of an emission barrier for electrons in the conduction band within NEA materials, the work function, ϕ, is substantially reduced. When incorporated into the Richardson-Dushman equation, this reduction leads to an exponential increase in emission current density at a given temperature, or equivalently, enables comparable emission at significantly lower temperatures. For diamond specifically, thermionic emission can occur at temperatures as low as ~800 °C while maintaining high current densities.[20]

Furthermore, the emission properties of diamond can be tailored through different surface terminations. Combined with its exceptional thermal stability and ability to sustain high current densities, NEA diamond is therefore a highly promising material for thermionic energy conversion applications, such as thermionic energy converters (TECs).[40]

1.7 Thermionic energy converters

Thermionic emission is widely utilised in solid-state devices such as thermionic energy converters (TECs) to convert thermal energy directly into electrical energy.[40] Figure 2 presents a schematic diagram of a TEC, comprising a heated emitter and a cooled collector, corresponding to the cathode and anode respectively, with different work functions. The two electrodes are separated by a vacuum gap. Upon heating, electrons are thermally excited, acquiring sufficient thermal energy to overcome the work function and are subsequently emitted from the cathode. The emitted electrons travel through the vacuum gap and are collected at the anode. This establishes a potential difference that drives an electrical current through the external circuit.[41]

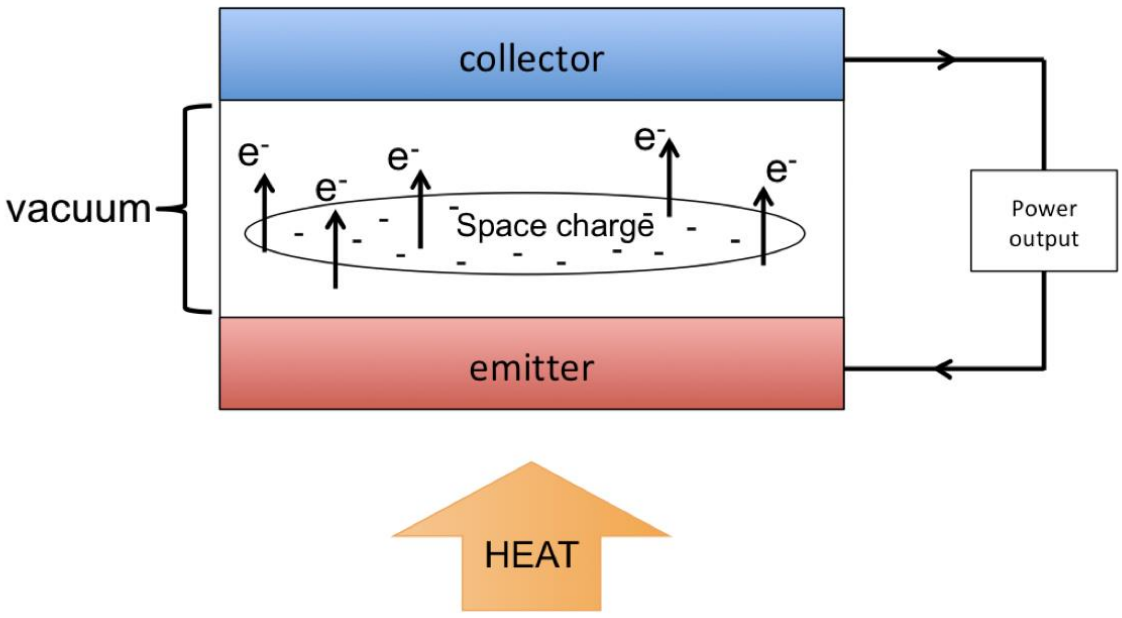

Figure 2 Schematic diagram for a thermionic energy converter device.[18]

TECs typically operate under vacuum conditions to minimise heat transfer between the electrodes and to enhance electron collection efficiency at the anode. From a thermodynamic perspective, a TEC operates as a heat engine, with the emitter and collector acting as hot and cold reservoirs, respectively. The maximum theoretical efficiency depends strongly on the temperature gradient between the two electrodes, as shown by the Carnot equation:[40–42]

Equation 4

$$\eta = 1 - \frac{T_{cold}}{T_{hot}}$$

In practice, the achievable efficiency is significantly reduced by space charge formation within the interelectrode gap and by radiative heat losses between the electrodes.

1.8 Surface terminations

NEA plays a crucial role in improving thermionic device performance and enabling alternatives to conventional cathode materials. Studies show surface functionalisation of diamond is a key strategy for enhancing NEA properties. A wide range of surface terminations has been explored over the years, including metal, hydroxyl, nitrogen-based species, oxygen and hydrogen.[20]

Among these, metal-based terminations have shown particularly promising results. Small, highly charged metal species such as Mg^{2+}, Al^{3+}, Ti^{4+}, and Sc^{3+} are especially effective because they readily ionise and form stable interactions close to the diamond surface. This proximity enhances both kinetic and thermal stability, which is beneficial for maintaining NEA under operating conditions. When metals interact with oxygen-terminated diamond surfaces, bonding can occur through ionic, covalent, or weaker dipolar interactions. In all cases, partial oxidation of the metal occurs, which suppresses further oxidation and improves the air stability of the surface.[20]

Non-oxygenated terminations are also of interest, particularly for achieving NEA more readily. Metals with electronegativity values below 2.6 are especially suitable, as they can induce NEA when deposited under ultra-high vacuum conditions. Overall, the choice of surface termination plays a critical role in determining both the electronic properties and stability of diamond, with metal-based systems offering a promising route for optimising performance in thermionic applications.[20]

1.8.1 Hydrogen Termination

Hydrogen termination is a straightforward and reliable method for generating NEA on diamond surfaces. It can be achieved directly through high-temperature hydrogen gas exposure,[43] hydrogen plasma treatment,[44] or polishing with diamond powder and olive oil,[45] or indirectly during CVD growth in a hydrogen-rich environment, resulting in an inherently H-terminated surface.[46] Structurally, hydrogen atoms bond to surface carbon atoms, preserving the (2 × 1) reconstruction on the (100) surface, while the (111) surface remains unreconstructed, as shown in Figure 3.[18]

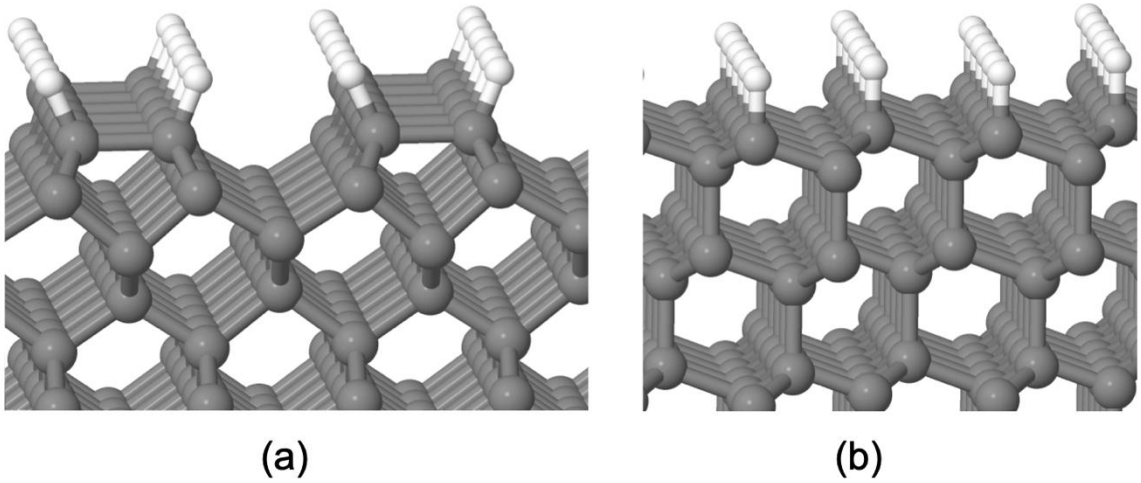

Figure 3 Simulations of the H-terminatied (a) (100) and (b) (111) diamond surfaces. Carbon and hydrogen atoms are shown in grey and white respectively.[18]

Hydrogenation significantly reduces surface resistivity via surface transfer doping, in which a redox reaction with atmospheric adsorbates such as moisture in air induces a two-dimensional hole gas (2DHG) with carrier densities on the order of 10^{12} - 10^{14} cm^{-2}.[47] This increases the diamond conductivity significantly, making H-terminated diamond attractive for electronic and catalytic applications, including electron emission in aqueous environments.

H-termination also provides a reliable experimental NEA ranging from approximately - 0.7 to - 1.3 eV for (100) and (111) surfaces respectively,[48–51] with computational values from density functional theory (DFT) calculations approaching -2 eV, which is close to the ideal value for efficient thermionic emission.[52–54]

The aforementioned properties enable thermionic emission at below 600 °C, significantly lower than conventional emission temperatures. In relation to the Richardson–Dushman equation, the thermionic emission current on H-terminated surfaces is achievable at significantly lower temperatures than on conventional emitters.[55]

However, the C-H bond is relatively weak, with an exothermic adsorption process and adsorption energies of -4.14 to -5.36 eV/atom on (100) and -4.37 eV/atom on (111) surfaces. This relatively low adsorption energy limits thermal robustness. Hydrogen begins to desorb at temperatures above ~500 °C, with significant loss occurring by ~700 °C. Its poor thermal and chemical stability leads to a transition from NEA to PEA, subsequently reducing emission

efficiency. Repeated thermal cycling further degrades emission current and increases the emission threshold. Additionally, exposure to air or water leads to gradual oxidation of the surface, which removes the NEA entirely over time.[56–58]

Overall, while hydrogen termination offers a convenient and effective route to achieving NEA and surface conductivity, its instability at elevated temperatures and under ambient conditions limits its long-term applicability. This has motivated the development of alternative terminations, particularly metal-functionalised surfaces, to improve stability and performance under practical operating conditions.

1.8.2 Oxygen termination

Oxygen termination of the diamond surface can be achieved through several oxidation methods, including oxygen plasma treatment, UV/ozone exposure, reaction with oxidants, and anodic polarisation. Two configurations can form on the oxidised surface: ether (C–O–C), in which oxygen bridges two carbon atoms, and ketone (C=O), in which oxygen is bonded to a single carbon. The type of bonding and surface coverage depend on crystallographic orientation and steric constraints, with partial monolayer coverage often favoured to minimise repulsion.[59,60]

On the (100) surface, both forms leave the surface structure unchanged, whereas on the (111) surface the existing (2 × 1) reconstruction is maintained. However, ketone formation breaks the surface carbon–carbon bond within the Pandey chain, as shown in Figure 4, leading to local structural modification.[18]

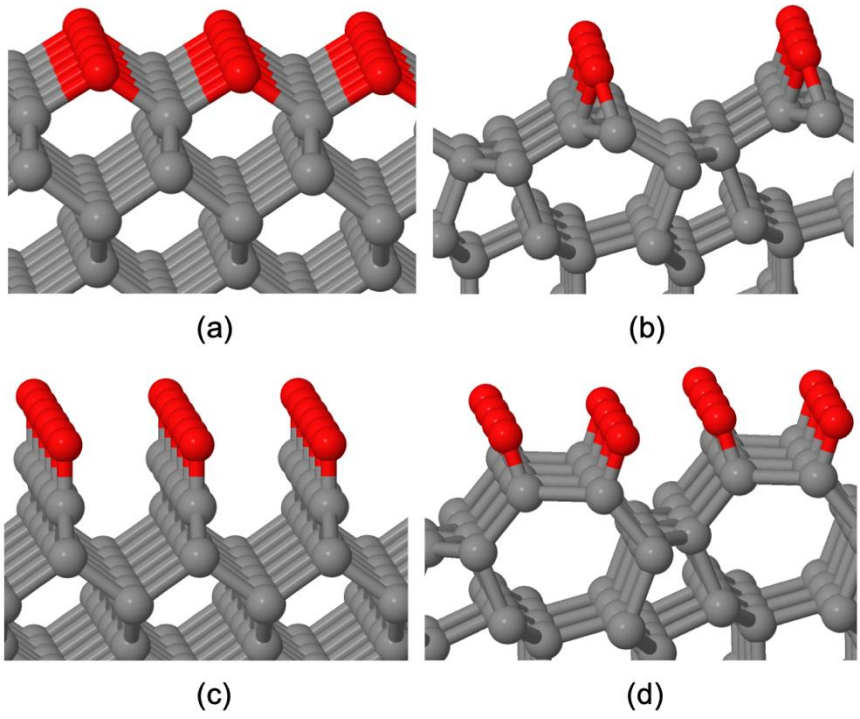

Figure 4 Simulations of the Simulations of the (a)–(b) ether O-terminated (100) and (111) diamond surfaces, respectively, and (c)–(d) the ketone O-terminated (100) and (111) diamond surfaces, respectively. C and O atoms are shown in grey and red, respectively.[18]

Computational studies predict that ether termination is slightly more energetically favourable than ketone termination, although it introduces lattice strain due to geometric mismatch. In practice, real surfaces are not ideal and may contain defects or edge sites, resulting in a mixture of bonding arrangements and making detailed characterisation challenging. Oxygen coverage is also dependent on termination configurations; ether termination corresponds to lower oxygen coverage whilst ketone termination corresponds to higher oxygen coverage. Theoretical studies suggest that intermediate coverage minimises repulsive interactions between adsorbates, although experimental work shows that higher coverages can still be achieved under specific conditions.[61]

Overall, oxygen-terminated diamond surfaces are structurally complex, with bonding configuration and coverage strongly influencing surface stability. Although oxygen termination is relatively stable with well-defined surface chemistry in comparison to other terminations, these surfaces generally exhibit PEA, with experimental values around 1.0 – 1.7 eV and theoretical values up to ~2.6 – 3.7 eV, making them unsuitable for thermionic emission.[62] Additionally, structural strain and surface heterogeneity complicate precise control and characterisation of the surface termination.[18]

1.8.3 Metal Termination

In comparison to other terminations, metal termination is one of the relatively simple approaches to achieving NEA on diamond surfaces. This method involves heating the diamond to remove any existing surface species, followed by deposition of a thin layer of low-electronegativity metal directly onto the clean diamond surface under ultra-high vacuum (UHV). Techniques such as evaporation, sputtering, or atomic layer deposition (ALD) are employed during this process.[20] Subsequently, an annealing step is performed to enable direct bonding of metal atoms to surface carbon atoms. The metal layer is usually kept at monolayer or sub-monolayer thickness to preserve surface-specific electronic properties.

This method enhances thermal robustness compared to hydrogen-terminated diamond. Experimental data show that diamond thin films with metal terminations such as Co, Cu, Zr, Ni, and Ti can exhibit NEA values in the range of 0.15 to 0.70 eV.[63–65] Theoretical studies indicate that metals capable of forming carbides with the carbon surface, such as Ti, V, and Al, show improvements in both surface stability and electron emission properties due to the strong metal–carbon bond. For instance, a very thin Ti layer (~3 Å) on nitrogen-doped diamond exhibits roughly doubles the thermionic emission current of a hydrogen-terminated surface, with higher binding energies (up to ~9.7 eV) and a favourable NEA value, owing to its high thermal stability at 950 °C.[66]

However, the electronic properties of a metal-terminated diamond surface are highly dependent on the exact metal coverage and atomic arrangement, making precise control particularly challenging. Metals such as copper, which do not readily form carbides, tend to show weaker NEA behaviour and may oxidise or desorb. In addition, achieving optimal performance requires very high temperatures and ultra-high vacuum, which is not always practical in device applications.[20,67]

1.8.4 Nitrogen Termination

Nitrogen surface terminations can be prepared using ammonia plasma treatment or by reacting chlorinated diamond with ammonia or methylamine, followed by further protonation using aqueous HCl to produce ammonium-terminated ($–NH_3^+$) surfaces.[67]

Due to nitrogen's trivalency, nitrogen-terminated diamonds exhibit a range of surface bonding configurations, including primary amines ($C–NH_2$), bridging secondary amines, and other functional groups such as imines and cyano species.[68] Although primary amine groups are the dominant species on nitrogenated diamond surfaces owing to their higher stability, other nitrogen configurations are still present.[69]

Nitrogen terminations are relatively straightforward to prepare and offer chemical versatility, allowing multiple functional surface states. However, purely nitrogenated surfaces, containing only carbon and nitrogen atoms tend to exhibit large positive electron affinity (PEA) values of 3.2 - 4.7 eV and relatively low stability, limiting their effectiveness for electron emission applications.[70]

Some nitrogen-containing surfaces can support photocatalytic nitrogen reduction and have been shown to exhibit a theoretical negative electron affinity (NEA) of approximately -0.7 ~ -0.8 eV on undoped diamond surfaces under both vacuum and aqueous conditions.[71] However, their properties are still significantly dependent on surface structure, coverage, and doping, leading to variability in reported electron affinities (ranging from -0.9 to +2.3 eV),[70] indicating strong sensitivity to local bonding environments. Furthermore, the coexistence of multiple bonding configurations makes it difficult to achieve well-defined and reproducible surface properties.

An extension of this approach involves bonding electropositive metals to nitrogenated surfaces, forming metal–nitrogen–diamond structures. For example, TiN-terminated diamond has been predicted to be more thermodynamically stable than simple amine terminations. Despite this, the calculated electron affinity ranges from −1.7 to +1.8 eV, which is less favourable than expected. While this approach may improve stability, it does not consistently enhance the NEA, and many potential metal–nitrogen systems remain unexplored.[70]

Overall, nitrogen termination offers flexibility and simple preparation, but it is limited by the instability in purely nitrogenated systems and variability in electronic properties. While metal–nitrogen hybrid structures can improve stability, their electron emission performance remains modest, indicating that further optimisation is required.[20]

1.8.5 Hydroxyl termination (C–OH)

Hydroxyl termination is a secondary process following the oxygenation of the diamond surface. It can be obtained via exposure to water vapour, where hydrogen acts as the electropositive species bound to surface oxygen, or via plasma treatments.[72]

Structurally, OH-termination favours reconstructed (2 × 1) surfaces on (100) diamond and unreconstructed (111) surfaces.[73] The electronic behaviour of hydroxyl-terminated diamond shows significant variability, with n-type systems displaying strongly positive electron affinity, reaching values as high as +4.3 eV.[20]

Computational studies predict that hydroxyl termination, achieved via hydrogen/oxygen plasma treatment on (100) diamond surfaces and via electrochemical oxidation on (111) surfaces, exhibits NEA in both cases. For the (100) surface, the predicted NEA ranges from approximately -0.55 to -2.13 eV,[52,53] with experimental values around -1.1 eV. The theoretical data make hydroxyl termination on diamond surfaces more promising for electron emission applications.[18] There is a lack of experimental confirmation of pure hydroxyl-terminated diamond as it is challenging to obtain a homogeneous hydroxylated surface without the coexistence of other oxygen functionalities.

One experimental approach solves this problem by using electrochemical treatment, in which the hydrogen-terminated diamond is subjected to high voltages in deionised water to generate hydroxide ions in situ.[74] Although this method demonstrates that full hydroxyl coverage is possible, it also leads to increased surface roughness, likely caused by the etching effects at high voltage. Such morphological changes introduce surface inhomogeneity, which may result in spatial variation in electronic properties such as electron affinity.

Overall, hydroxyl termination offers potential for achieving NEA, and the surface hydroxyl groups provide a platform for further functionalisation, including silanisation, polymer grafting, and biomolecule attachment. This further functionalisation enables potential applications in biosensors and photocathodes. However, its practical implementation is limited by difficulties in producing smooth, homogeneous surfaces and by the strong dependence of its electronic properties on surface structure and doping.

Yoshida et al. recently proposed a promising approach to achieving full OH-termination on the diamond (111) surface via water vapour annealing, notably without inducing surface etching.[75]

In this approach, H-terminated diamond is annealed in a water vapour atmosphere at 500 °C by flowing nitrogen through deionised water. At this temperature, a significant increase in sheet resistivity has been reported, as degradation of the C–H bonds leads to the disappearance of the surface two-dimensional hole gas. FTIR analysis confirms this chemical transformation, showing the loss of C–H features and the emergence of C–O–H bonding, with no indication of other oxygen terminations. Most importantly, atomic force microscopy reveals that the surface remains atomically flat following treatment, with no increase in roughness or evidence of etching.[75] This contrasts with conventional methods, which typically degrade surface morphology. These findings demonstrate that water vapour annealing enables selective formation of OH-terminated diamond while preserving surface integrity, making it a promising approach for controlled surface modification in electronic applications. However, there is a lack of XPS data demonstrating OH-termination surface coverage.

1.9 General Project Aim

This project aims to commission and utilise a newly installed high-temperature tube furnace, capable of heating substrates up to 1000 °C under controlled atmospheric conditions, to investigate whether complete hydroxyl (OH) termination can be achieved on single-crystal diamond surfaces.

This study aims to replicate and further evaluate the theory and experimental procedure reported by R. Yoshida et al.,[75] who recently demonstrated the formation of atomically flat hydroxyl-terminated single-crystal diamond surfaces through water vapour annealing of hydrogen-terminated diamond. Although Fourier transform infrared spectroscopy (FTIR) measurements presented in their study indicated successful OH termination, the authors did not quantify the surface coverage percentage achieved in this procedure.

The first stage of this project will, therefore, involve commissioning the tube furnace. This will include assembly of the gas flow-through system, with assistance from Dr. James Smith, followed by leak testing using both dry and moist nitrogen gas to ensure a sealed and stable operating environment. The furnace will then be tested under a range of temperatures and ramping conditions without diamond samples, to confirm reliable and safe operation.

Once the furnace has been confirmed to operate consistently and safely, single-crystal diamond substrates will undergo high-temperature water vapour annealing under a series of controlled temperature conditions.

Following treatment, the samples will be characterised using the University of Bristol nanoESCA facility. Techniques including X-ray photoelectron spectroscopy (XPS), ultraviolet photoelectron spectroscopy (UPS), and photoemission electron microscopy (PEEM) will be utilised to quantify the extent of OH termination, as well as to determine the work function and negative electron affinity (NEA) of the treated diamond surfaces.

The experimental aim is to achieve complete hydroxyl (OH) coverage of the diamond surface while determining the optimal temperature conditions required for this process.

2.1 Commissioning the tube furnace

The tube furnace, as shown in Figure 5, was set up with generous help from Professor Paul May and Dr James Smith. A water bubbler and an N_2 gas line were connected to the inlet of the tube furnace, each independently controlled via a valve. During operation, N_2 passed through the tube furnace and exited via the outlet into the atmosphere.

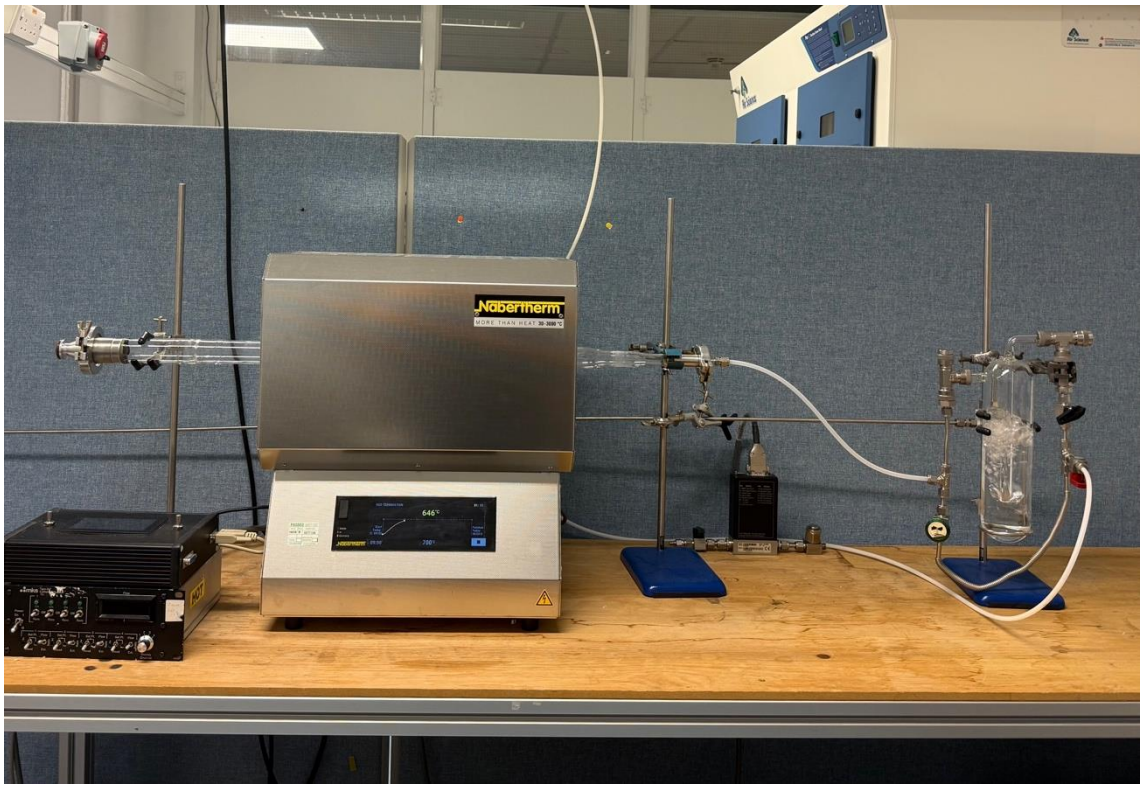

Figure 5 Tube Furnace connected with nitrogen gas and a water bubbler.

A schematic diagram of the tube furnace gas flow is shown in Figure 6. Dry N_2 passes through the water bubbler, resulting in moist N_2 entering the tube furnace. Upon reaction, the valve connecting the N_2 line to the water bubbler was closed, allowing dry N_2 to pass directly into the tube furnace.

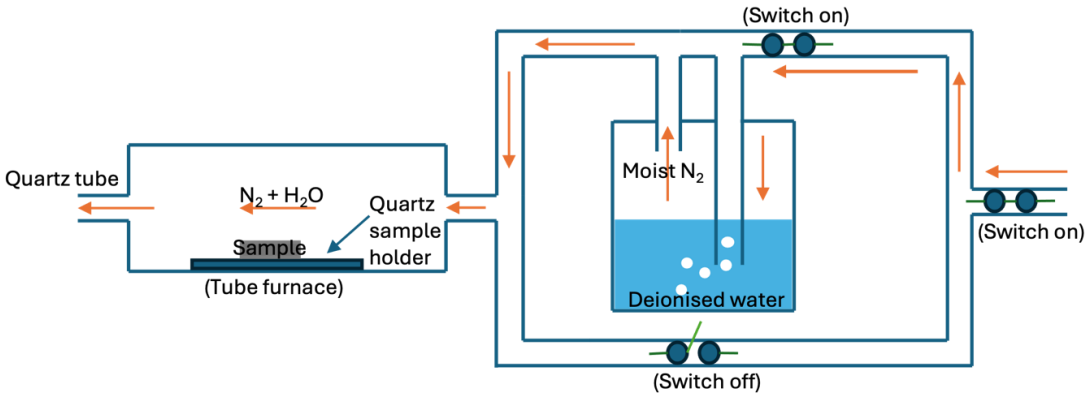

Figure 6 Schematic diagram of the tube furnace.

2.2 Acid Cleaning

To remove surface impurities from the diamond, an acid clean was carried out with assistance from Dr. Ramiz Zulkharnay. In a round-bottom flask, five 3 x 3 mm single-crystal chemical vapour deposition (CVD) (100) diamond plates were combined with 100 mL of sulfuric acid (95%) with 6.5 g of KNO3 and refluxed for three hours at 220 °C. The colourless liquid turned lemon yellow as the temperature rose. After reflux, the mixture was left to cool to room temperature before being diluted with deionised water. The solution was discarded while the diamonds were placed in a beaker with sufficient acetone. The mixture was left to sonicate for 15 minutes.

2.3 Laser etching

A small circle was etched on a corner of one side of the CVD diamond plate using an Oxford Lasers system, shown in Figure 7, to distinguish the front side from the back side.

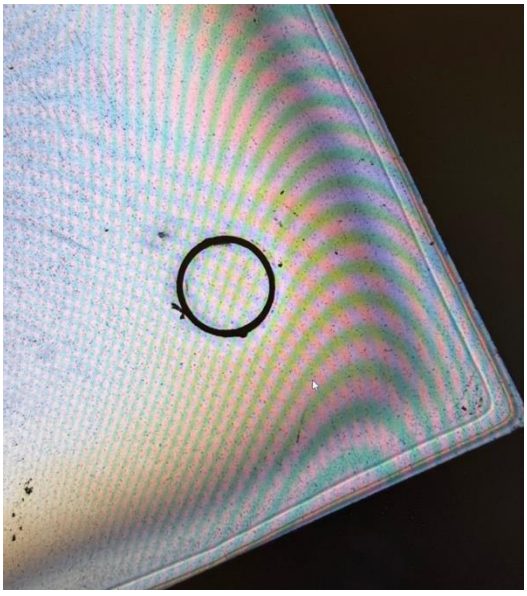

Figure 7 Diamond surface post laser etching.

2.4 Boron doping

A thin (0.5 μm) boron-doped layer was grown epitaxially on the front side (the side without the laser-etched marking) in a microwave reactor, a 3 kW microwave plasma system with a substrate area of about 2 cm^2 which can grow boron doped diamond at up to 20 μm h^{-1},[76] shown in Figure 8, diamond samples during treatment shown in Figure 9. This ensured that the diamond surfaces were electrically conducting so that the samples did not charge up during XPS analysis of the OH-terminated surfaces.

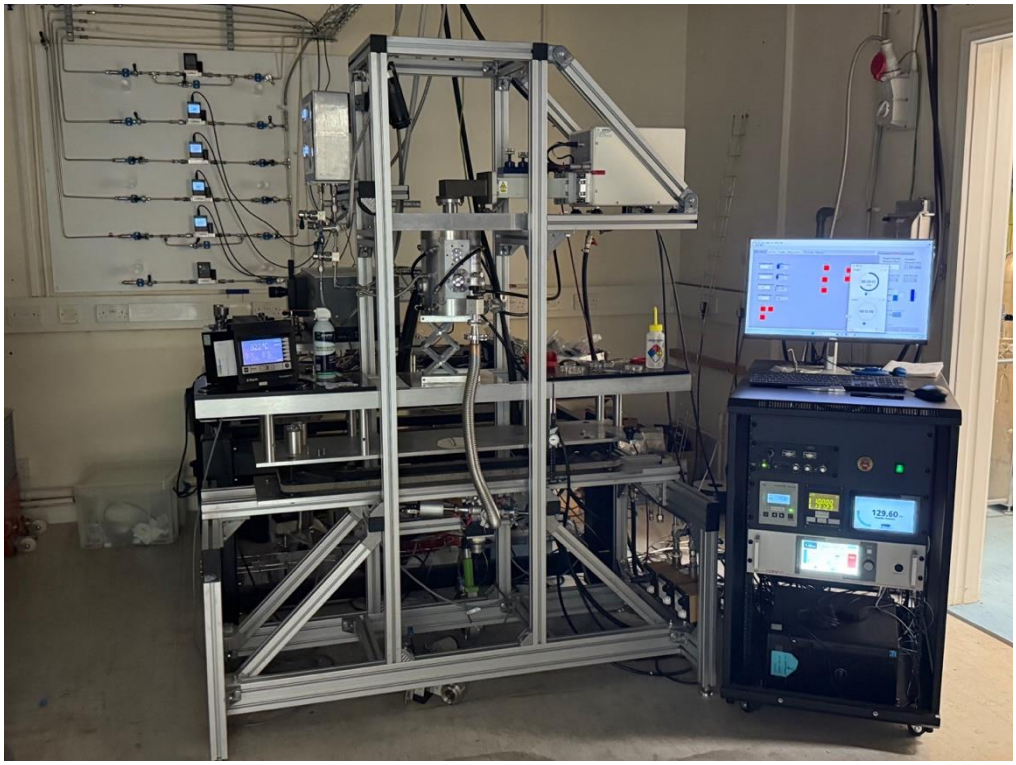

Figure 8 Microwave reactor used in Boron doping and hydrogen termination.

Figure 9 Diamond samples within the MW reactor chamber.

2.5 Hydrogen termination

After the boron doping, the samples remained in the microwave reactor in pure H_2 for 10 minutes.

2.6 Hydroxyl termination

A single-crystal CVD diamond plate was placed on a quartz holder, as shown in Figure X. The quartz holder was gently inserted into the tube furnace using a long metal rod. The nitrogen gas flow and water bubbler were both turned on, allowing a steady flow of moist nitrogen through the tube furnace throughout the procedure. The tube furnace was set to ramp to 700 °C and held under moist N_2 at 700 °C for one hour to ensure uniform treatment. Upon completion, the tube furnace was set to cool naturally, the water bubbler was switched off, and dry N_2 was allowed to flow through until the tube furnace reached 200 °C. This ensured that oxygen and carbon-containing molecules in air did not interfere with the hot CVD diamond plate or disrupt the termination on the diamond surface while hot. The sample was then carefully removed and stored in an N_2 - purged vial sealed with parafilm to prevent air exposure.

Four samples, M1, M2, M3, and M4 were treated following the same procedure at different temperature conditions (700 °C, 900 °C, 700 °C, and 500 °C, respectively) for a comparative study of temperature-dependent effects on their properties.

2.7.1 X-ray Photoelectron Spectroscopy (XPS)

X-ray photoelectron spectroscopy (XPS) is a surface-sensitive technique performed under ultra-high vacuum (UHV), in which a material is irradiated with X-rays, causing photoelectron emission. The kinetic energy E_K of these electrons is measured using a hemispherical analyser, as shown in Figure 10, allowing the binding energy E_B to be determined from:

Equation 5

$$E_B = h\nu - E_K - \phi$$

where $h\nu$ is the photon energy and ϕ is the spectrometer work function. Variations in binding energy, known as chemical shifts, arise from changes in oxidation state and local electronic environment, reflecting differences in bonding and charge distribution.[77]

In this report, XPS is used to analyse the chemical composition and bonding states of diamond films. It is particularly useful for distinguishing between different carbon bonding states, as shifts in binding energy reflect variations in electronic structure associated with different forms of carbon. The measured binding energies are also influenced by relaxation effects following photoemission. XPS is inherently surface sensitive, as only electrons originating from the top ~10 nm of the material can escape without significant energy loss due to their short inelastic mean free path (~0.5–2 nm).[77] Thus, XPS provides information on the near-surface region of diamond thin films, which is essential for understanding the surface chemistry and termination performance.

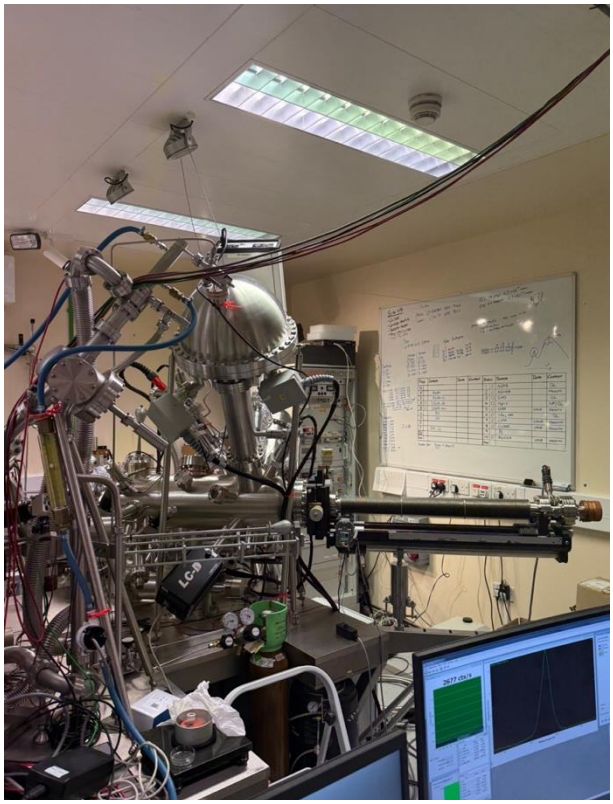

Figure 10 X-ray Photoelectron Spectroscopy (XPS)

2.7.2 Ultraviolet Photoelectron Spectroscopy (UPS)

Similar to XPS, ultraviolet photoelectron spectroscopy (UPS) is a surface-sensitive technique that also relies on photoirradiation leading to photoelectron emission.[78] In this technique, ultraviolet radiation on a material surface results in the ejection of valence electrons, rather than core-level electrons as in XPS. It is primarily used to determine the electronic structure of materials, especially within the valence band region, ionisation energies and the surface work function.[79] The work function (Φ) can be determined from the UPS spectrum using the following equation:

Equation 6

$$\Phi = h\nu - w$$

Where *hv* corresponds to the photon energy and *w* corresponds to the spectral width between the Fermi level and the secondary electron cutoff, assuming the alignment between the Fermi level of the sample and the spectrometer.

UPS is highly surface sensitive as the emitted electrons are low in kinetic energy, which corresponds to a minimum in the inelastic mean free path. Thus, the detected signal originates from only the top few atomic layers, with a typical sampling depth of ~10–20 Å. According to the Beer–Lambert law shown in Equation 7, the signal intensity decreases exponentially with depth.

Equation 7

$$I = I_0 e^{-d/\lambda}$$

The UPS work mechanism can be demonstrated using a three-step model as shown in Figure 11. The incident photons can excite electrons from the valence band to energies above the vacuum level (E_{vac}), producing a distribution reflecting the valence band structure. As a result, these excited electrons migrate towards the material surface. While some electrons reach the surface retaining their original energy distribution without losing any energy, others undergo inelastic scattering, losing the kinetic energy gained and subsequently contributing to the formation of secondary electrons, spanning energies from the Fermi level (E_F) to above the vacuum level. The Fermi level corresponds to that of the spectrometer and sample holder, and alignment with the sample Fermi level is only ensured when electrical equilibrium is established. In experimental procedures, helium discharge sources are commonly used, providing photon energies at 21.22 eV (He I) and 40.81 eV (He II), which enable high energy resolution. However, due to surface charging effects, UPS is not a suitable technique for analysing insulating materials.[79]

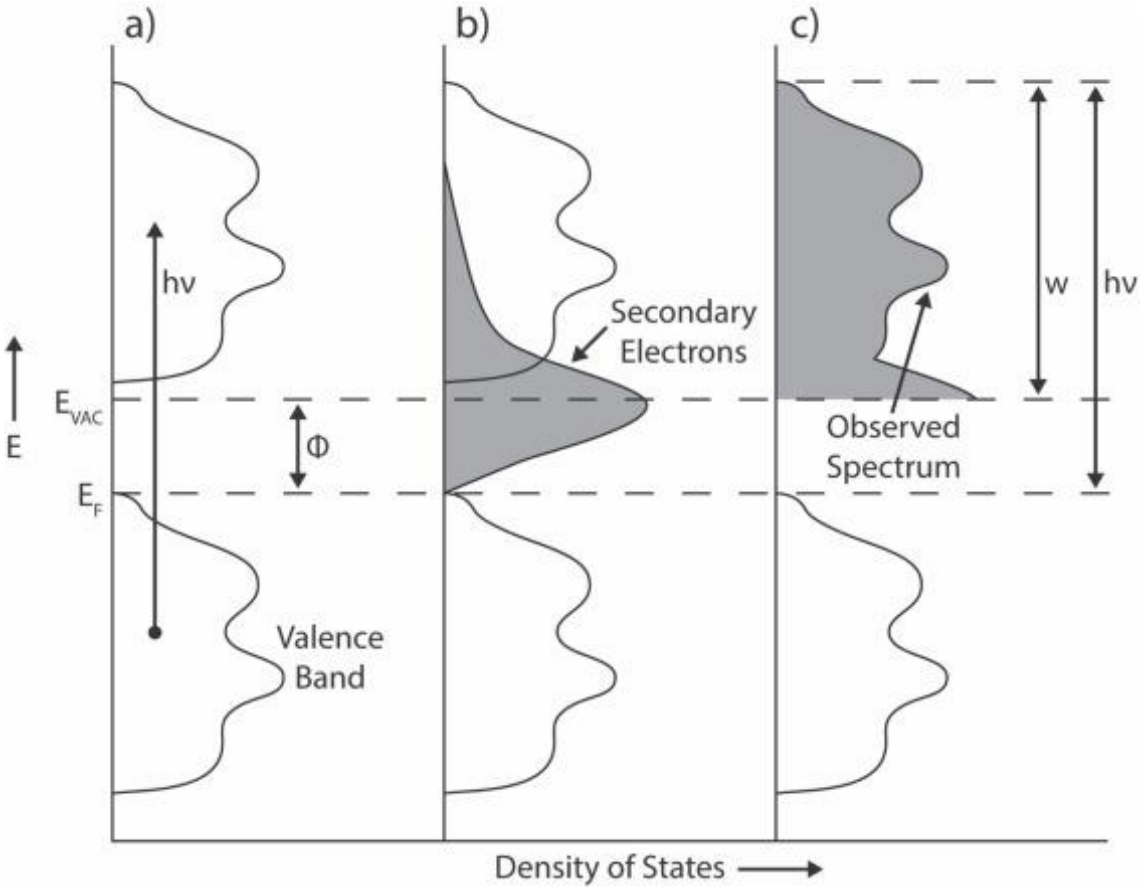

Figure 11 Three step work mechanism of UPS.[79]

2.7.3 Photoemission Electron Microscopy (PEEM)

Photoemission electron microscopy (PEEM) is a surface-sensitive imaging technique that generates contrast from photoelectrons emitted following irradiation. Developed in the 1930s, it is related to Low Energy Electron Microscopy (LEEM) and Spin-Polarised Low Energy Electron Microscopy (SPLEEM), but unlike these techniques, PEEM uses photoionised electrons and is not restricted to crystalline samples.[80]

PEEM offers strong surface sensitivity and elemental specificity, making it well suited for studying ultra-thin films, multilayers, and alloys. It is also capable of detecting antiferromagnetic order, which distinguishes it from many other magnetic imaging methods. The spatial resolution is typically 30–100 nm, placing it between transmission electron microscopy and optical techniques such as Kerr microscopy. In a typical setup, as shown in Figure 12, synchrotron radiation is used as the excitation source. X-rays are polarised, dispersed by a grating, and monochromatised before illuminating the sample. The use of tunable, polarised radiation allows different contrast mechanisms to be selected, enabling PEEM to function as a spectromicroscopy technique.[80]

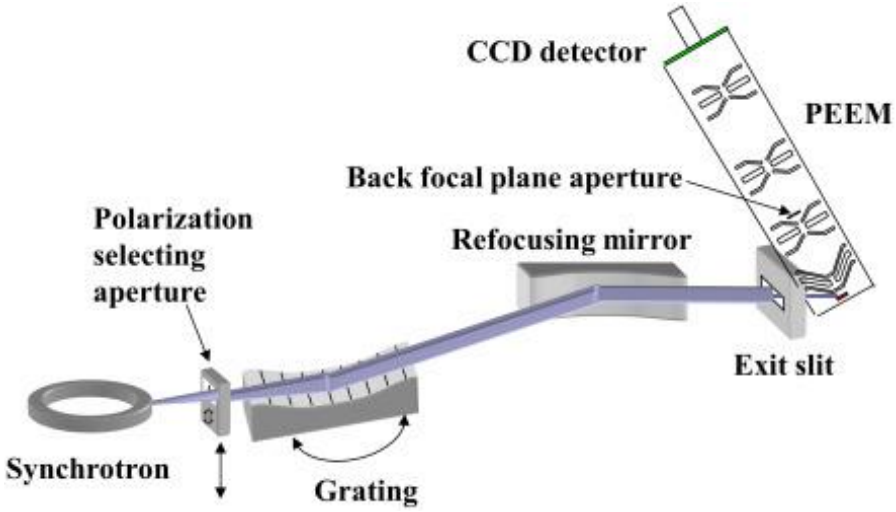

Figure 12 Typical set up of PEEM.[80]

3.1 Fourier Transform Infrared (FTIR) Spectroscopy Characterisation

The OH-termination on the (111) diamond surface reported by R. Yoshida et al. utilised FTIR as a primary analytical technique. To ensure consistency with the literature, FTIR analysis was performed on Samples M1 and M2. Based on the literature, successful hydroxyl termination on the diamond surface via water annealing is identified by the presence of a C-OH absorption band in the range ~850 – 1125 cm^{-1}, following the disappearance of the C-H stretching at ~2837 cm^{-1} and the absence of other oxygen-related vibrational modes.[75]

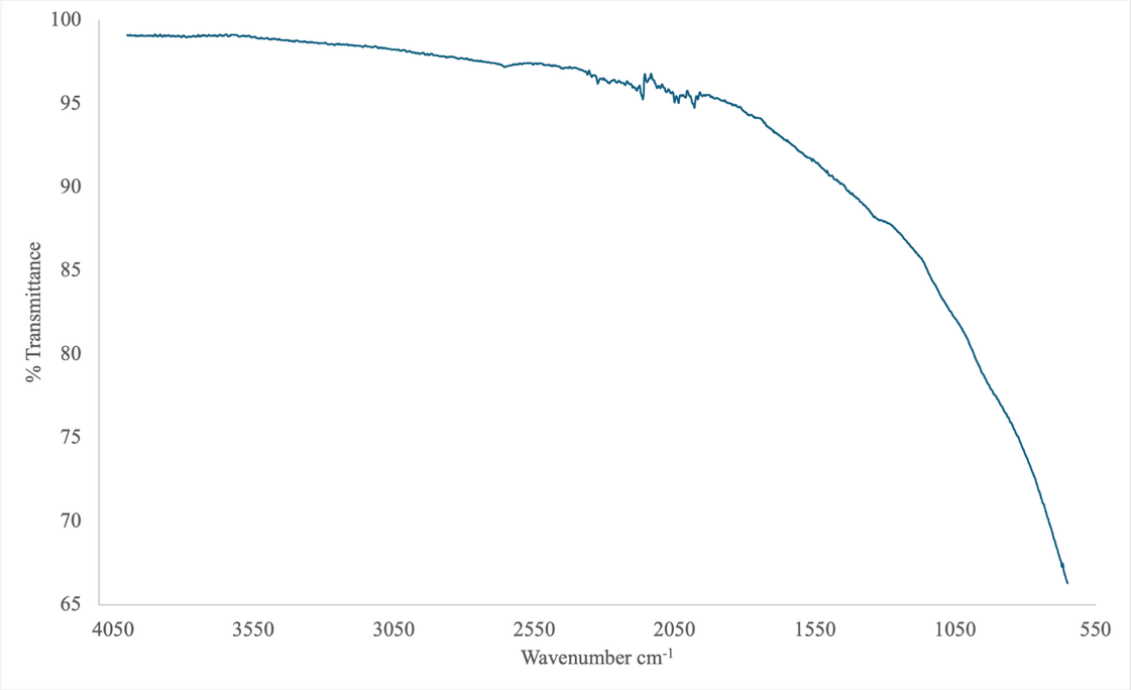

Figure 13 FTIR spectrum for Sample M1 – treated at 700 °C.

The FTIR spectrum for Sample M1, as shown in Figure 13, is dominated by a broad transmittance decrease with no well-defined absorption peaks. There is no distinct absorption observed in the C-H bond stretching region (~ 3000 – 2800 cm^{-1}), however, due to the lack of a reference spectrum prior to hydroxyl termination, it is not possible to confirm the disappearance of C-H bonds. A weak feature is present at ~2100 – 2000 cm^{-1}, which lies within the range typically associated with nitrile (C≡N) bond stretching.[81] However, given the termination temperature at 700 °C, nitrile bond formation is not feasible. This feature is therefore more likely to be caused by diamond surface defects or instrumental noise. Overall, there are no significant vibrational modes that can be clearly identified, and the spectrum does not provide definitive evidence for the presence of any surface functional groups.

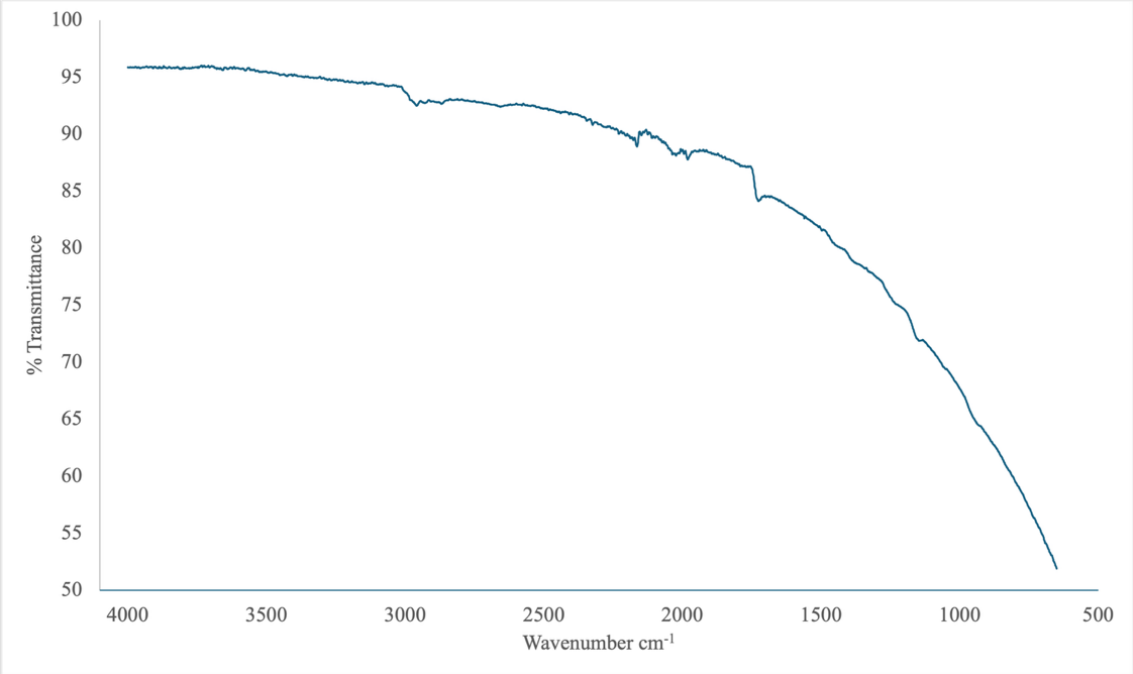

Figure 14 FTIR spectrum for Sample M1 – treated at 900 °C.

The FTIR spectrum for Sample M2 as shown in Figure 14, shows similar characteristics with a broad transmittance decrease with no well-defined absorption peaks. A weak, low intensity feature is visible around ~2200 cm^{-1} corresponding to the nitrile stretching region[81]. However, due to the lack of a sharp and well-defined peak, nitrile formation cannot be conclusively assigned. Given that this treatment was carried out at 900 °C, a high enough temperature to make a nitrile-related feature chemically plausible, this assignment cannot be confirmed by the data. No distinct C-H or C=O stretching bands are observed, and no specific surface functional groups can be definitively identified from this spectrum.

The experimental FTIR spectra for Samples M1 and M2 show very limited agreement with the literature spectrum reported by Yoshida et al. Neither spectrum displays a clearly resolved C-OH band in the ~850 – 1125 cm^{-1} region comparable to that reported in the literature. Furthermore, the absence of a clear reference prevents the confirmation of successful C-H bond removal. Thus, successful hydroxyl termination cannot be confirmed from the FTIR data alone. While Sample M2 may show slightly stronger evidence of nitrile formation compared to Sample M1, neither spectrum provides conclusive proof of nitrile formation.

Therefore, although the spectra may suggest some degree of surface modification, they are unable to reproduce the clear FTIR behaviour reported in literature. Although FTIR is widely used in characterisation of surface chemistry, its usefulness for assessing diamond surface termination is limited in this case. The possible reflection effects arising from a diamond-on-diamond measurement, combined with the strong contribution from the diamond substrate, make it difficult to isolate weak surface-specific vibrational features. The strong baseline and lack of surface-specific bands indicate that FTIR provides very limited evidence for diamond surface termination, making it unreliable for definitive assignment, and the data should therefore be interpreted cautiously.

3.2 X-ray Photoelectron Spectroscopy (XPS) Characterisation

3.2.1 Survey Scan

Following the high temperature water annealing of CVD diamond samples to obtain OH-terminated surface, XPS survey scan analysis was performed on all four samples, M1 – M4. The survey spectra obtained are shown in Figure 15.

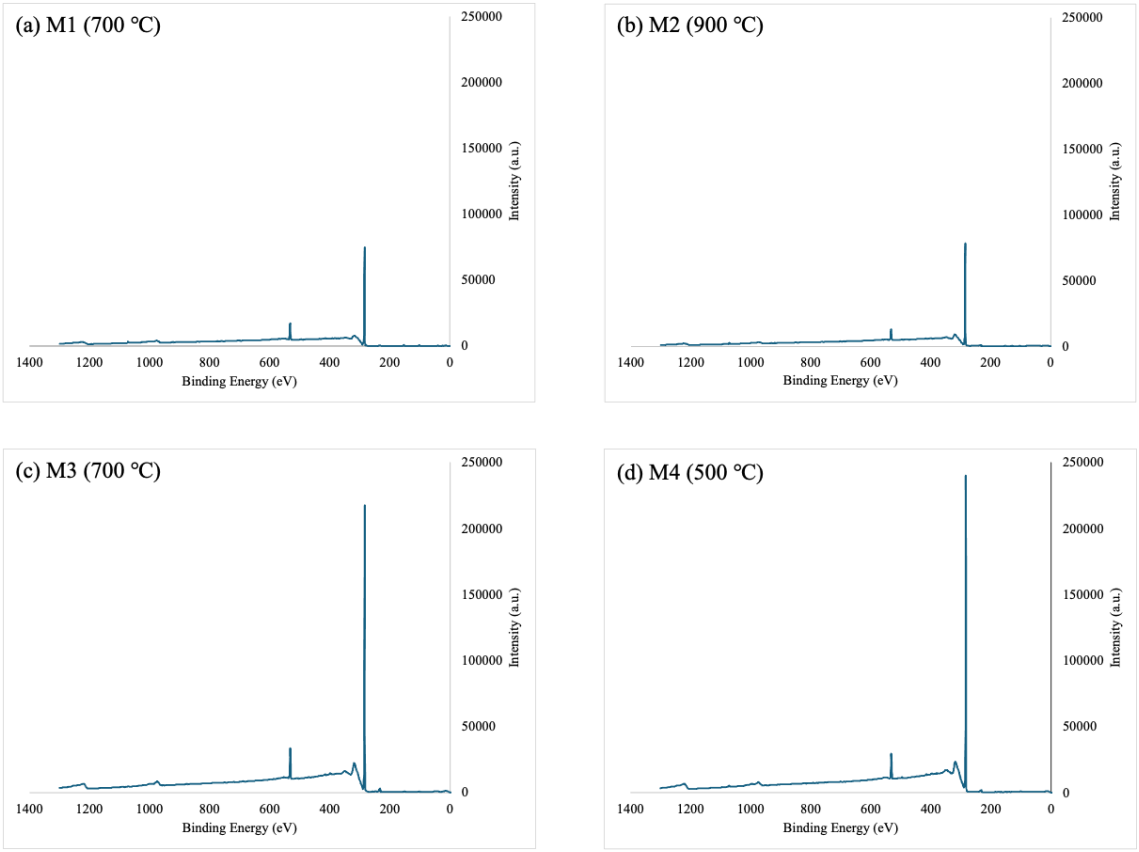

Figure 15 X-ray Photoelectron Spectroscopy (XPS) Survey scan, (a) M1, 700 °C, (b)M2, 900 °C, (c) M3, 700 °C, (d) M4, 500 °C.

All four samples exhibit a dominant C1s peak at approximately 285 eV; this corresponds to the literature value for sp^3 hybridised carbon on diamond surfaces.[82] Within all spectra, an O1s signal is also detected in the range of 530 – 535 eV, corresponding to literature values for oxygen-containing surface species associated with OH-termination.[82] Additionally, weak features observed at approximately 950 – 1000 eV are present in all four spectra, attributed to the C KLL Auger transition, a key characteristic of carbon-rich materials.

There are no obvious additional elemental peaks observed, indicating the absence of significant detectable surface contamination from the sample holder or surrounding environment. The strong intensity of the carbon signal across all spectra indicates that the analysed surface is predominantly diamond.

Although XPS survey scans are not typically used for precise quantitative chemical analysis, they can allow for qualitative comparison of relative elemental contributions.

A key distinction between the samples is the relative intensity of the O1s peak. Sample M4, treated at 500 °C demonstrates the strongest relative O1s intensity amongst the four, indicating greater retention of oxygen-containing surface groups. In contrast, Sample M2, treated at 900 °C, demonstrates the weakest relative O1s signal, consistent with the thermal decomposition of oxygen-containing groups at elevated temperatures.

Samples M1 and M3 were both treated at under the sample temperature conditions at 700 °C and displayed broadly similar spectral features with strong C1s peaks and intermediate oxygen intensities. This indicates partial loss of surface oxygen post annealing. However, Sample M3 appears to show a stronger overall carbon intensity than M1, which may arise from variations in sample positioning, surface area exposed to the X-ray beam, or even local surface morphology.

In conclusion, the survey spectra confirm that all four samples remain carbon-dominated and retain detectable oxygen species after treatment. A clear temperature-dependent trend is observed, with decreasing O1s intensity as annealing temperature increases from 500 °C to 900 °C. Indicating progressive thermal loss of oxygen-containing surface species, consistent with the dihydroxylation of the OH-terminated diamond surface.

Further insight into the carbon and oxygen bonding environments will require high-resolution analysis of the C1s and O1s regions.

3.2.2 C1s Scan

The XPS C1s scans for Samples M1 – M4 were obtained. The binding energy (BE) was determined using Equation X, where *hv* is the photon energy (1486.7 eV for Al Kα radiation) and KE is the measured kinetic energy of the emitted electron.

Equation 8

$$\boldsymbol{BE = hv - KE}$$

The resulting spectra were plotted as binding energy versus relative intensity and peak fitting was performed using XPS 4.1 software. The percentage surface coverage of each species was calculated from its relative peak area using Equation 9, where $A_{species}$ represents the fitted peak area of the species of interest and ΣA_{total} is the sum of the peak areas of all identified species. The calculated surface coverages are presented in Table 1.

Equation 9

$$\textbf{Surface coverage } (\%) = \frac{\boldsymbol{A_{species}}}{\sum \boldsymbol{A_{total}}} \times \mathbf{100}$$

Table 1

Sample	Temp (°C)	C-C (sp^3) ~284.4 eV (%)	C-O / C-OH ~285.0 eV (%)	C=O / O-C=O ~286.5 - 288.5 eV (%)
M1	700	68.9	29.1	1.9
M2	900	87.8	8.3	3.9
M3	700	52.7	46.8	0.5
M4	500	57.7	41.1	1.2

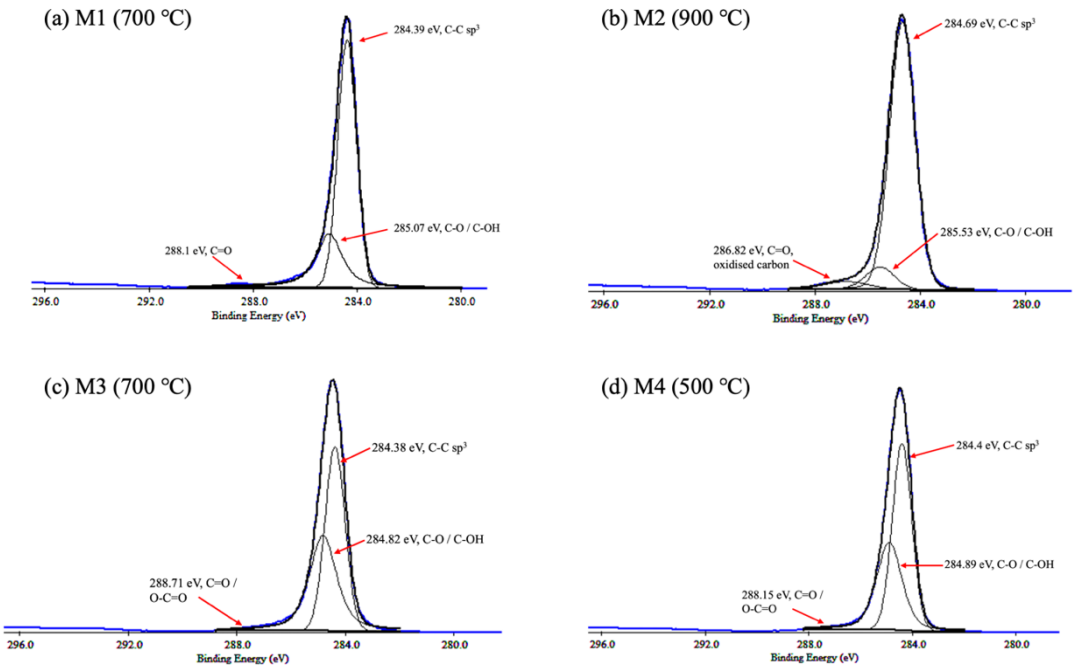

Figure 16 X-ray Photoelectron Spectroscopy (XPS) C1s scan, (a) M1, 700 °C, (b)M2, 900 °C, (c) M3, 700 °C, (d) M4, 500 °C

The analysed C1s spectra shown in Figure 16 and the quantified percentage surface coverages shown in Table 1 enable a detailed comparison of the surface chemistry across Samples M1 – M4. From these data, clear variations in chemical composition as a function of water annealing temperature can be observed.

In all samples, the dominant peak within the range of 284.3 – 284.7 eV is assigned to sp^3 hybridised C-C bonding,[83] corresponding to literature values and confirming the preservation of the diamond lattice. However, the relative contribution of this component and the extent of higher binding energy features vary significantly between samples.

For Sample M1, treated at 700 °C (Figure 16 (a)), the peak at 284.39 eV corresponds to sp^3 hybridised C-C bonding, dominating the spectrum with a surface coverage of 69.0%. There is a substantial secondary contribution at 285.07 eV (29.2%) corresponding to C-O / C-OH or defect associated carbon. A minor component at 288.1 eV (1.9%) corresponds to higher oxidation states, such as C=O / O-C=O. Overall, Sample M1 retains predominantly diamond-like surface features with measurable oxygen-related functionality.

In contrast, Sample M2, treated at 900 °C (Figure 16 (b)) exhibits markedly higher sp3 hybridised C-C bonding at 284.69 eV (87.8 %), accompanied by a significant reduction in oxygen containing species. The C-O / C-OH and oxidised carbon components show a percentage surface coverage of 8.3 % and 3.9 % respectively, both diminished relative to Sample M1. This result indicates that higher temperature annealing promotes surface oxygen species removal, yielding a cleaner and more homogeneous surface.

Interestingly, Sample M3, despite being treated under the same temperature conditions as Sample M1, exhibits different surface coverage components. As shown in Figure 16 (c), the sp^3 hybridised C-C contribution decreases to 52.7 % with a large overlapping feature at 284.4

eV (46.8 %), which corresponds to C-O / C-OH bonding or surface disorder. However, its close proximity to the major peak illustrates partial peak broadening rather than fully resolved chemical states. This indicates significantly greater surface modification compared to Sample M1, which is likely to be influenced by variations in surface defects or local surface structure.

Similarly, Sample M4, treated at 500 °C (Figure 16 (d)) also demonstrates a reduced sp3 hybridised C-C coverage (57.7 %), alongside a secondary component (41.1 %) associated with oxygen containing or disordered carbon species and a minor oxidised contribution (1.2 %).[83] These results suggest that lower temperature treatment favours the retention of oxygen-containing surface species.

In conclusion, the C1s spectra demonstrate a clear temperature dependence of surface chemistry, with higher annealing temperatures reducing oxygen related contributions and enhancing surface sp^3 character. The disparity between Samples M1 and M3 further highlights the influence of surface specific factors beyond temperature.

3.2.3 O1s Scan

The O1s spectra were analysed following the same aforementioned procedure. The fitted spectra are shown in Figure 17, and the corresponding percentage surface coverages are summarised in Table 2.

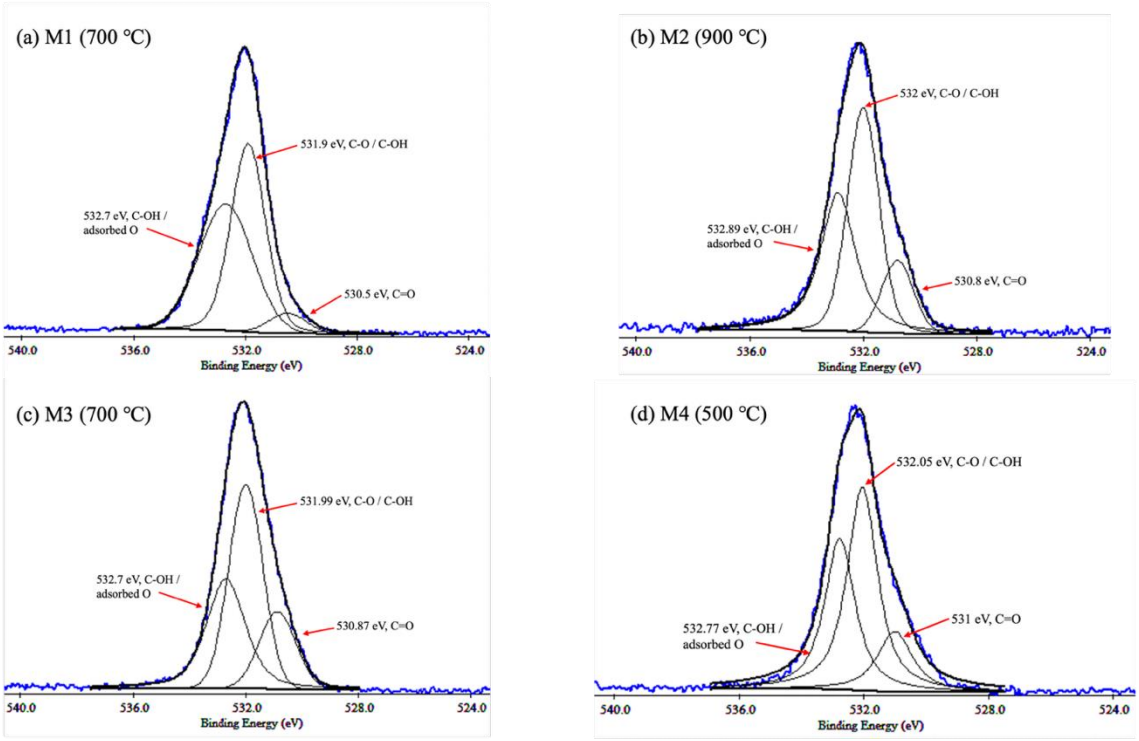

Figure 17 X-ray Photoelectron Spectroscopy (XPS) O1s scan, (a) M1, 700 °C, (b)M2, 900 °C, (c) M3, 700 °C, (d) M4, 500 °C

Table 2

Sample	Temp (°C)	C=O ~530.8 eV (%)	C-O / C-OH ~532.0 eV (%)	C-OH / adsorbed O ~532.7 - 532.9 eV (%)
M1	700	5.3	48.3	46.4
M2	900	14.1	45.9	39.9
M3	700	19.0	46.2	34.8
M4	500	16.6	47.7	35.7

The O1s spectra shown in Figure 17 provide further insight into the oxygen containing functionalities present on Samples M1 – M4 following thermal treatment. Each spectrum was deconvoluted into three principal components, corresponding to lower binding energy oxygen species (C=O), C-O / C-OH environments and higher binding energy species such as hydroxyl groups, adsorbed oxygen, as well as weakly bound water-like species.[83]

For Sample M1, treated at 700 °C, shown in Figure 17 (a), the O1s spectrum is dominated by two peaks at 531.90 eV (48.3 %) and 532.70 eV (46.4 %), representing C-O / C-OH and higher binding energy oxygen species respectively. A minor peak at 530.50 eV (5.3 %) indicates carbonyl or more strongly bonded oxygen species, confirming a significant oxygen containing surface contribution.

In contrast, Sample M2, treated at 900 °C, shown in Figure 17 (b) exhibits an increase in the C=O component (14.2 %), demonstrating a greater proportion of more strongly bound or carbonyl-like oxygen species. Although present in reduced quantities, the remaining contributions at 532.00 eV (46 %) and 532.89 eV (39.9 %) still indicate the presence of oxygen and potentially in more stable configurations compared to Sample M1.

For Sample M3, in contrast to the C1s results, the O1s spectrum is more consistent with Sample M1. Strong contributions from C-O / C-OH (46.2 %) and higher binding energy species (34.8 %) are observed, alongside a relatively large lower binding energy component (19.0 %). This demonstrates substantial oxygen incorporation and a slightly higher degree of surface functionalisation relative to Sample M1.

Similarly, Sample M4, treated at 500 °C, as shown in Figure 17 (d), exhibits a dominant component at 532.05 eV (47.7 %) and a significant higher binding energy contribution (35.7 %), indicating a strong retention of oxygen-containing species. The lower binding energy component of 16.6 % further supports the presence of a mixture of different oxygen environments.

To conclude, the O1s spectra confirm the presence of oxygen-containing surface species in all samples, with a clear dependence on annealing temperature. While peaks at approximately 532 eV correspond to C-O / C-OH environments, the overlap between oxygen species limits definitive peak assignment, and the reported components should therefore be considered indicative rather than absolute.

The combined C1s and O1s analysis confirms that all samples retain a predominantly sp^3 hybridised diamond surface upon thermal treatment, with varying degrees of oxygen containing surface functionality. In particular, the components assigned to C-O / C-OH in the C1s spectra and species at approximately 532 eV in the O1s spectra are consistent with the presence of hydroxyl related surface species.

Sample M2 (900 °C) exhibits the highest sp3 hybridised carbon content and the lowest relative contribution from oxygen containing species, indicating that while high temperature annealing promotes the removal of surface functionalities and produces a comparatively clean surface, this high temperature condition is not favourable for achieving OH-termination on the CVD diamond surface.

In contrast, Samples M3 and M4 show significantly higher oxygen associated species, suggesting greater retention of surface functional groups, while Sample M1 represents an intermediate case.

Despite the identical treatment temperatures, the disparity between Samples M1 and M3 highlights the influence of surface specific factors, such as defect density on the diamond surface or surface morphology, on the extent of surface functionalisation. Overall, lower annealing temperatures favour the retention of oxygen containing species.

Though, owing to the overlap between contributions from C-O, C-OH and other oxygen containing species in both the C1s and O1s spectra, definitive identification of hydroxyl termination cannot be confirmed using XPS alone. Additional complementary techniques would therefore be required alongside XPS for unambiguous confirmation. Nevertheless, the results demonstrate that thermal treatment provides an effective means of tuning diamond

surface chemistry, with conditions that favour increased oxygen incorporation while being consistent with the enhanced hydroxyl related surface functionality.

3.3 Ultraviolet Photoelectron Spectroscopy (UPS) Characterisation

Ultraviolet photoelectron spectroscopy (UPS) was utilised to probe the electronic structure of Samples M3 and M4. It is capable of providing information on the work function, valence band structure, and the valence band maximum (VBM) of a material. The full spectra (Figure 18) show the distribution of photoemitted electrons as a function of binding energy (E-EF), with peaks observed at higher binding energies (~ 15 – 17 eV) and a broader peak around approximately 8 – 10 eV, corresponding to deeper electronic states and the valence band states respectively.

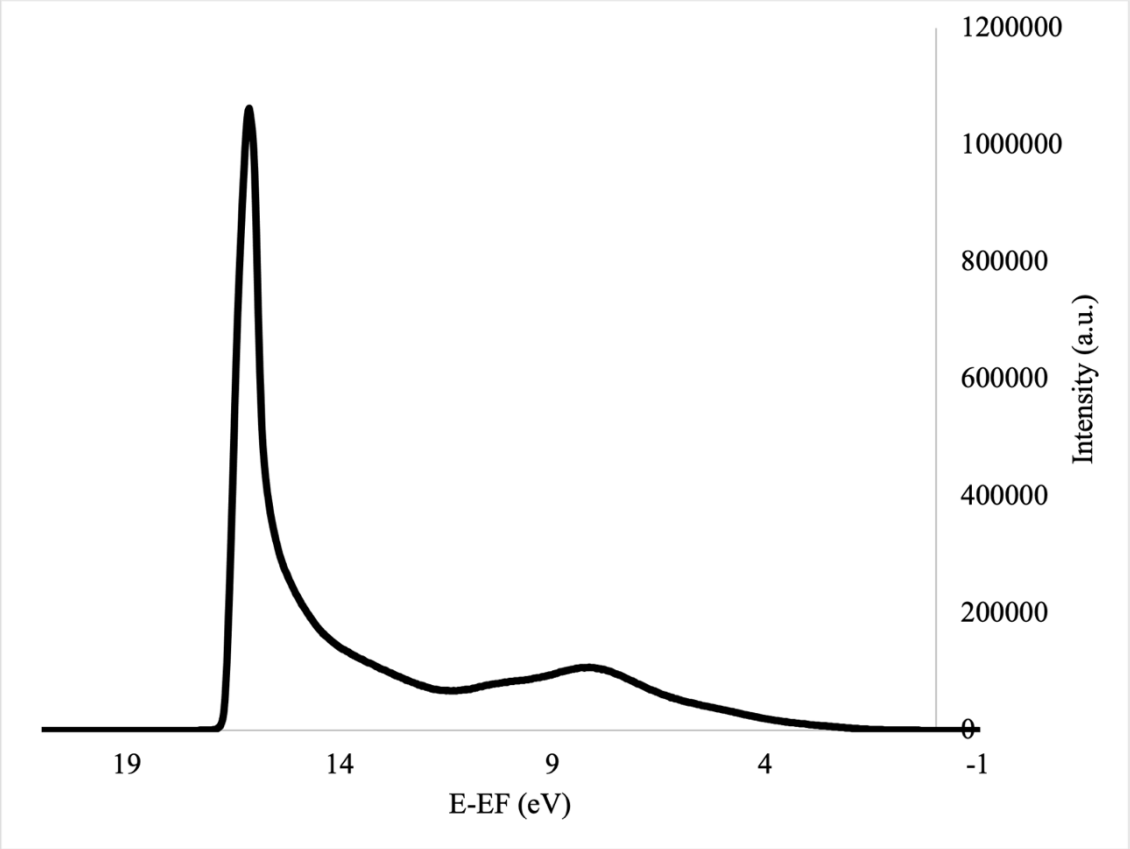

Figure 18 Ultraviolet photoelectron spectroscopy (UPS) spectra for Sample M3.

A magnification of the low binding energy region, 0 – 10 eV, shown in Figure 19 reveals that there is no distinct valence band near the Fermi level, preventing the determination of the valence band maximum (VBM).

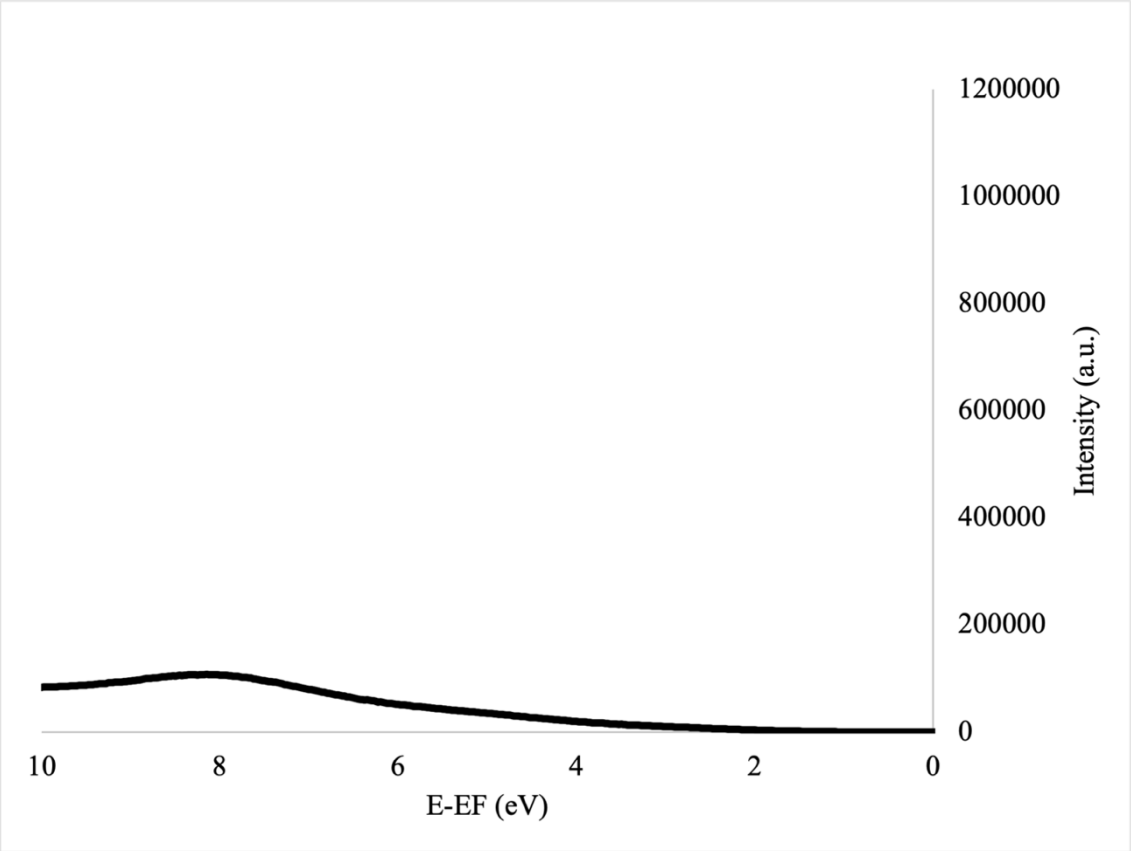

Figure 19 Magnification of the low binding energy region, 0 – 10 eV of Sample M3 UPS.

During the measurement, the sample exhibited significant charging under UV illumination. This behaviour results in local variations in the electrostatic potential, leading to energy-scale shifts and substantial broadening of spectral features. These factors obscures the true electronic structure near the Fermi level and therefore, prevents accurate identification of the VBM.

Furthermore, charging-induced distortion makes the extraction of absolute energetic parameters unreliable. In particular, the work function of the material could not be determined, as the available dataset does not contain a secondary electron cutoff and is affected by energy-scale shifts.

As with Sample M3, the UPS analysis of the M4 surface reveals a highly similar profile (Figure 20), with pronounced features at higher binding energies (~ 15 – 17 eV) and a broader peak around approximately 8 – 10 eV.

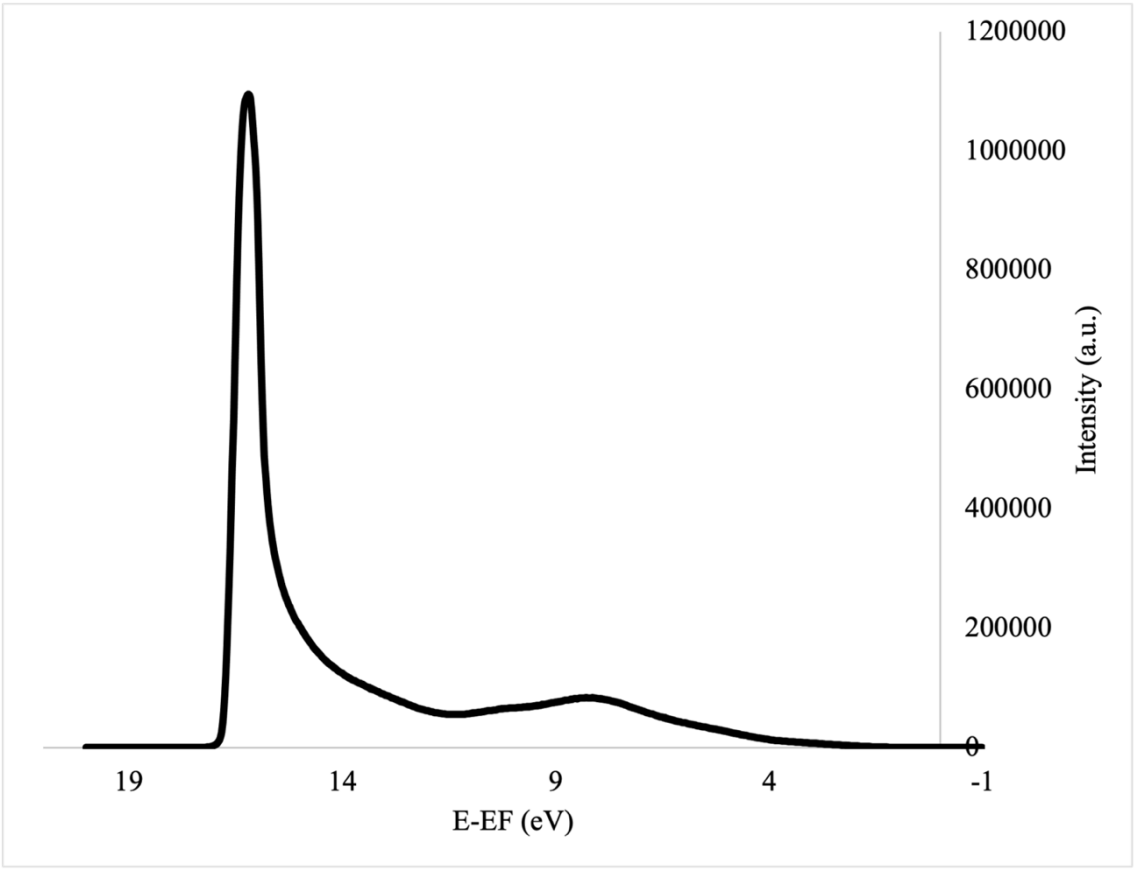

Figure 20 Ultraviolet photoelectron spectroscopy (UPS) spectra for Sample M4.

The magnification of the low binding energy region 0 – 10 eV, once again shows a gradual decrease in intensity towards the Fermi level without a clear linear onset, preventing reliable extraction of the VBM. This observed behaviour is once again attributed to the sample charging during measurement.

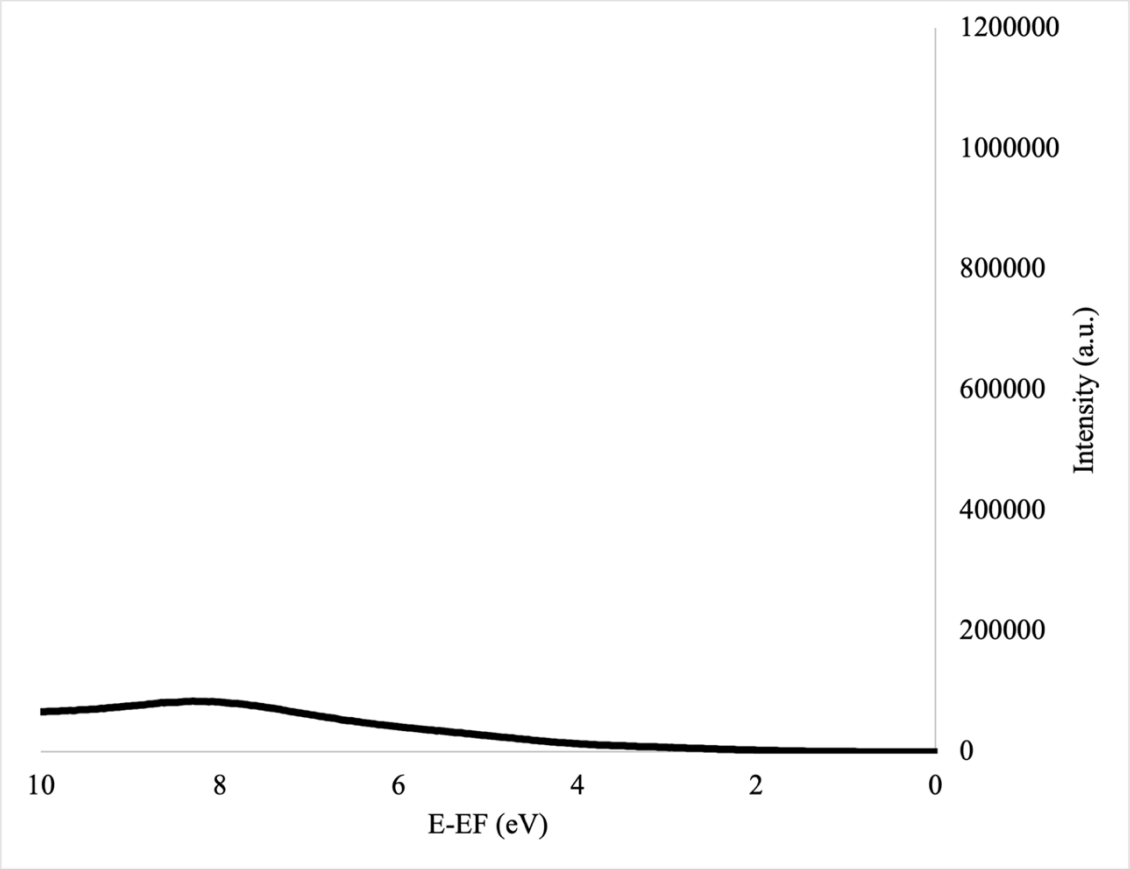

Figure 21 Magnification of the low binding energy region, 0 – 10 eV of Sample M4 UPS.

In conclusion, the UPS analysis for both Samples M3 and M4 provides qualitative insight into the valence electronic structure, with consistent features observed across both samples. However, significant sample charging under UV illumination severely limited the ability to extract quantitative parameters, such as the valence band minimum (VBM), work function, and band gap. While the spectra suggest plots consistent with wide bandgap or insulating materials, definitive conclusions regarding absolute electronic structure cannot be drawn. As a result, reliable determination of the work function would be required to assess the changes in surface termination, including the potential hydroxyl functionalisation on CVD diamond surfaces. Further measurements employing improved charge compensation, such as optical spectroscopy or inverse photoemission would be required to obtain reliable quantitative data.

4. Conclusion

This project has successfully commissioned a high-temperature tube furnace. It was utilised for a controlled modification of single-crystal diamond surfaces via a water vapour annealing process, with the aim of achieving a complete hydroxyl (OH) terminated surface and evaluating its suitability for advanced electron emission applications.

The tube furnace system demonstrated reliable, leak-free operation under controlled atmospheric conditions and enabled reproducible high-temperature treatments at temperatures ranging from 500 °C – 900 °C. This has provided a robust experimental apparatus for investigating the temperature-dependent surface functionalisation of CVD diamond.

Comprehensive surface characterisation using FTIR, XPS and UPS revealed that all treated samples retained a predominantly sp^3 hybridised carbon structure. This confirms the preservation of the diamond lattice following thermal treatment. All spectra of XPS analysis consistently identified oxygen-containing surface species, with a clear inverse relationship between annealing temperature and oxygen content.

Lower-temperature treatments, particularly at 500 °C, resulted in significantly higher relative contributions from oxygen species, whereas higher temperatures (900 °C) promoted substantial removal of these species, yielding a more chemically reduced and homogeneous surface. High-resolution C1s and O1s spectra indicated the presence of C-O and C-OH related environments on the diamond surface, demonstrating the presence of partial hydroxylation. However, despite these encouraging indications, quantitative determination of hydroxyl surface coverage was precluded by the inherent overlap between oxygen functionalities in XPS spectra, and complete OH termination was not achieved.

FTIR analysis failed to resolve the characteristic C-OH vibrational modes as reported in literature. This is likely caused by intrinsic sensitivity limitations and substrate interference in diamond systems.

UPS measurements were similarly inconclusive, as severe sample charging obscured key electronic features, preventing accurate determination of the work function, valence band maximum (VBM) and the assessment of negative electron affinity (NEA).

While the results highlight that water vapour annealing is an effective route for introducing oxygen-based functionalities, achieving controlled and homogeneous hydroxyl termination remains challenging.

For samples treated under identical conditions, the observed differences further emphasise the significant role of surface-specific factors, such as defect density, surface morphology, and local bonding environment. This illustrates that temperature alone is insufficient as a controlling parameter for diamond surface chemistry.

In the context of the broader project aim, this study provides valuable experimental insight into the challenges associated with engineering diamond surfaces for optimised electron emission. While complete OH termination could not be conclusively demonstrated, the findings support the hypothesis that lower temperature water vapour annealing favours hydroxyl related surface species and represents a viable pathway towards NEA enabled surfaces.

Overall, this work establishes a strong experimental foundation for further optimisation of diamond surface termination and contributes meaningfully to the development of thermally robust, low-work-function materials for next-generation thermionic energy conversion technologies.

5. Future work

While this study provides a solid experimental foundation for hydroxyl-terminated diamond surfaces produced via water vapour annealing, there are several key areas requiring further development in order to fully achieve the project aim of a well characterised, fully OH-terminated CVD diamond surface.

An important priority is the implementation of more definitive characterisation techniques. The limitations encountered using FTIR and UPS analysis highlighted the need for higher-sensitivity, more surface-specific methods. Future work should therefore incorporate synchrotron-based XPS or UPS to improve resolution and signal-to-noise ratio, alongside other techniques capable of distinguishing between closely related oxygen functionalities, such as near-edge X-ray absorption fine structure (NEXAFS)[84] or high-resolution electron energy loss spectroscopy (HREELS).[85] In addition, angle-resolved XPS could provide further insight into surface coverage and depth distribution of OH species.[86]

Sample charging during UPS measurements should also be addressed; in this study, it significantly limited the extraction of reliable electronic parameters. This could be resolved through improved conductive pathways, such as optimised boron doping, reduced insulating regions, or the use of charge compensation systems (e.g. electron flood guns). Determining a reliable work function is essential for evaluating NEA, a key requirement for diamond applications in thermionic emission devices.

The water vapour annealing process parameters could be optimised further to achieve a controlled and reproducible hydroxyl termination. This study explored only the temperature variation in water vapour annealing; future work should investigate additional variables including annealing time, water vapour concentration, gas flow rate and system pressure. Greater control over these parameters may enable selective hydroxyl group formation while suppressing competing oxygen species such as carbonyls.

The variation observed between samples treated under identical conditions suggests that surface functionalisation is strongly dependent on the initial surface state, including defect density, roughness, and pre-existing terminations.

Future studies could therefore focus on more rigorous and standardised pre-treatment protocols, as well as incorporating detailed imaging using atomic force microscopy (AFM) or scanning electron microscopy (SEM), prior to annealing to allow correlation of initial surface quality with final termination.

To better align this research with electronic applications, future research should aim to establish a clear relationship between surface termination and electron emission properties. This includes reliable measurement of work function, electron affinity, and emission current density, potentially through direct thermionic emission testing. Such studies would provide a more complete evaluation of the compatibility of OH-terminated diamond in thermionic energy conversion.

Finally, building on the findings of Yoshida et al., further work should focus on quantifying OH surface coverage, which remains a critical gap in both this study and existing literature. The development of a reliable methodology for quantification will be essential for validating the success of hydroxyl termination methodologies.

In conclusion, future work should aim to focus on integrating improved characterisation techniques, tighter process control, and direct functional testing. This combined approach will be crucial to advance from qualitative observation of surface modification to reliable engineering of diamond surfaces with tailored electronic properties for high-performance thermionic application.

6. References

1 A. C. Li, B. Li, F. González-Cataldo, R. E. Rudd, B. Militzer, E. M. Bringa and M. A. Meyers, Diamond under extremes, *Elsevier Ltd*, 2024, preprint, DOI: 10.1016/j.mser.2024.100857.

2 R. Zulkharnay and P. W. May, Applications of diamond films: a review, *Functional Diamond*, DOI:10.1080/26941112.2024.2410160.

3 T. Stachel and J. W. Harris, Formation of diamond in the Earth's mantle, *Journal of Physics: Condensed Matter*, 2009, **21**, 364206.

4 D. Das, in *Carbon-Based Nanofillers and Their Rubber Nanocomposites*, Elsevier, 2019, pp. 123–181.

5 R. J. Narayan, R. D. Boehm and A. V. Sumant, in *Diamond-Based Materials for Biomedical Applications*, Elsevier, 2011, pp. 3–24.

6 Diamond history and Lore.

7 J. E. Butler and A. N. Katrusha, in *Diamond: Genesis, Mineralogy and Geochemistry*, De Gruyter, 2023, pp. 689–754.

8 S. S. Dossa, I. Ponomarev, B. N. Feigelson, M. Hainke, C. Kranert, J. Friedrich and J. J. Derby, Analysis of the High-Pressure High-Temperature (HPHT) growth of single crystal diamond, *J. Cryst. Growth*, 2023, **609**, 127150.

9 K. Luo, B. Liu, W. Hu, X. Dong, Y. Wang, Q. Huang, Y. Gao, L. Sun, Z. Zhao, Y. Wu, Y. Zhang, M. Ma, X.-F. Zhou, J. He, D. Yu, Z. Liu, B. Xu and Y. Tian, Coherent interfaces govern direct transformation from graphite to diamond, *Nature*, 2022, **607**, 486–491.

10 J. Zhang, J. Wang, G. Zhang, Z. Huo, Z. Huang and L. Wu, A review of diamond synthesis, modification technology, and cutting tool application in ultra-precision machining, *Mater. Des.*, 2024, **237**, 112577.

11 Performance and characterisation of CVD diamond coated, sintered diamond and WC–Co cutting tools for dental and micromachining applications.

12 H. Pedersen and S. D. Elliott, Studying chemical vapor deposition processes with theoretical chemistry, *Theor. Chem. Acc.*, 2014, **133**, 1476.

13 B. V. Spitsyn, L. L. Bouilov and B. V. Derjaguin, Vapor growth of diamond on diamond and other surfaces, *J. Cryst. Growth*, 1981, **52**, 219–226.

14 P. Bou, L. Vandenbulcke and R. Herbin, Plasma diamond deposition from CH4□H2(□O2□Ar) in relation to kinetic calculations, *Diam. Relat. Mater.*, 1992, **1**, 933–944.

15 R. J. Nemanich, Growth and Characterization of Diamond Thin Films, *Annual Review of Materials Science*, 1991, **21**, 535–558.

16 B. W. Paul M, *Diamond thin films: a 21st-century material*, 2000, vol. 358.

17 B. M. Nichols, J. E. Butler, J. N. Russell and R. J. Hamers, Photochemical functionalization of hydrogen-terminated diamond surfaces: A structural and mechanistic study, *Journal of Physical Chemistry B*, 2005, **109**, 20938–20947.

18 M. C. James, *Aluminium and Oxygen Termination of Diamond for Thermionic Applications*, 2019.

19 C. Wild, R. Kohl, N. Herres, W. Miiller-Sebert and P. Koidl, *Oriented CVD diamond films: twin formation, structure and morphology*, 1994.
20 4. A review of surface functionalisation of diamond for thermionic emission applications.
21 T. I. Awan, A. Bashir, A. Tehseen and S. Bibi, in *Chemistry of Nanomaterials*, Elsevier, 2020, pp. 179–206.
22 R. H. Fowler and L. Nordheim, Electron emission in intense electric fields, *Proceedings of the Royal Society of London. Series A, Containing Papers of a Mathematical and Physical Character*, 1928, **119**, 173–181.
23 H. E. EXNER, in *Physical Metallurgy*, Elsevier, 1996, pp. 943–1032.
24 P. J. Wilbur, R. G. Jahn and F. C. Curran, Space electric propulsion plasmas, *IEEE Transactions on Plasma Science*, 1991, **19**, 1167–1179.
25 V. L. Granatstein, R. K. Parker and C. M. Armstrong, Vacuum electronics at the dawn of the twenty-first century, *Proceedings of the IEEE*, 1999, **87**, 702–716.
26 M. W. Geis, J. C. Twichell, N. N. Efremow, K. Krohn and T. M. Lyszczarz, Comparison of electric field emission from nitrogen-doped, type Ib diamond, and boron-doped diamond, *Appl. Phys. Lett.*, 1996, **68**, 2294–2296.
27 P. W. May, J. C. Stone, M. N. R. Ashfold, K. R. Hallam, W. N. Wang and N. A. Fox, The effect of diamond surface termination species upon field emission properties, *Diam. Relat. Mater.*, 1998, **7**, 671–676.
28 J. B. Cui, J. Ristein, M. Stammler, K. Janischowsky, G. Kleber and L. Ley, Hydrogen termination and electron emission from CVD diamond surfaces: a combined secondary electron emission, photoelectron emission microscopy, photoelectron yield, and field emission study, *Diam. Relat. Mater.*, 2000, **9**, 1143–1147.
29 A. Siddique, A. Akram and Y. Jamil, in *Modern Luminescence from Fundamental Concepts to Materials and Applications*, Elsevier, 2023, pp. 51–84.
30 M. Shur, in *The Electrical Engineering Handbook*, Elsevier, 2005, pp. 153–162.
31 *Wide Bandgap Semiconductors : Fundamental Properties and Modern Photonic and Electronic Devices*, Elsevier Science, 1993.
32 G. Vergara, A. Herrera-Gómez and W. E. Spicer, Calculated electron energy distribution of negative electron affinity cathodes, *Surf. Sci.*, 1999, **436**, 83–90.
33 O. Romanyuk, I. Bartoš, I. Gordeev, A. Artemenko, M. Varga, T. Ižák, M. Marton, P. Jiříček and A. Kromka, Electron affinity of undoped and boron-doped polycrystalline diamond films, *Diam. Relat. Mater.*, 2018, **87**, 208–214.
34 S. Dushman, Electron Emission from Metals as a Function of Temperature, *Physical Review*, 1923, **21**, 623–636.
35 O. W. Richardson, LXVII. The distribution of the molecules of gas in a field of force, with applications to the theory of electrons, *The London, Edinburgh, and Dublin Philosophical Magazine and Journal of Science*, 1914, **28**, 633–647.
36 F. A. M. Koeck and R. J. Nemanich, Advances in Thermionic Energy Conversion through Single-Crystal n-Type Diamond, *Front. Mech. Eng.*,
37 F. A. M. Koeck and R. J. Nemanich, Substrate-diamond interface considerations for enhanced thermionic electron emission from nitrogen doped diamond films, *J. Appl. Phys.*,
38 J. F. Morris and D. L. Jacobson, *THERMIONIC ENERGY CONVERSION FOR SPACE-POWER AND TERRESTRIAL-TOPPING APPLICATIONS A BRIEF BACKGROUND OF THERMIONIC ENERGY CONVERSION*, 1964.
39 G. N. Hatsopoulos and J. Kaye, Measured Thermal Efficiencies of a Diode Configuration of a Thermo Electron Engine, *J. Appl. Phys.*, 1958, **29**, 1124–1125.

40 F. Huffman, in *Encyclopedia of Physical Science and Technology*, Elsevier, 2003, pp. 627–638.
41 K. A. Abdul Khalid, T. J. Leong and K. Mohamed, Review on Thermionic Energy Converters, *IEEE Trans. Electron Devices*, 2016, **63**, 2231–2241.
42 J. M. Houston, Theoretical Efficiency of the Thermionic Energy Converter, *J. Appl. Phys.*, 1959, **30**, 481–487.
43 T. Ando, M. Ishii, M. Kamo and Y. Sato, Thermal hydrogenation of diamond surfaces studied by diffuse reflectance Fourier-transform infrared, temperature-programmed desorption and laser Raman spectroscopy, *Journal of the Chemical Society, Faraday Transactions*, 1993, **89**, 1783.
44 J. van der Weide and R. J. Nemanich, Argon and hydrogen plasma interactions on diamond (111) surfaces: Electronic states and structure, *Appl. Phys. Lett.*, 1993, **62,** 1878–1880.
45 J. S. Hovis, S. K. Coulter, R. J. Hamers, M. P. D'Evelyn, J. N. Russell and J. E. Butler, Cycloaddition Chemistry at Surfaces: Reaction of Alkenes with the Diamond(001)-2 × 1 Surface, *J. Am. Chem. Soc.*, 2000, **122**, 732–733.
46 K. Kimura, K. Nakajima, S. Yamanaka, M. Hasegawa and H. Okushi, Hydrogen analysis of CVD homoepitaxial diamond films by high-resolution elastic recoil detection, *Nucl. Instrum. Methods Phys. Res. B*, 2002, **190**, 689–692.
47 F. Maier, M. Riedel, B. Mantel, J. Ristein and L. Ley, Origin of Surface Conductivity in Diamond, *Phys. Rev. Lett.*, 2000, **85**, 3472–3475.
48 C. Bandis and B. B. Pate, Photoelectric emission from the negative electron affinity (100) diamond surface — exciton effects, *Surf. Sci.*, 1996, **350**, 315–321.
49 C. Bandis and B. B. Pate, Photoelectric emission from negative-electron-affinity diamond (111) surfaces: Exciton breakup versus conduction-band emission, *Phys. Rev. B*, 1995, **52**, 12056–12071.
50 J. B. Cui, J. Ristein and L. Ley, Electron Affinity of the Bare and Hydrogen Covered Single Crystal Diamond (111) Surface, *Phys. Rev. Lett.*, 1998, **81**, 429–432.
51 F. Maier, J. Ristein and L. Ley, Electron affinity of plasma-hydrogenated and chemically oxidized diamond (100) surfaces, *Phys. Rev. B*, 2001, **64**, 165411.
52 S. J. Sque, R. Jones and P. R. Briddon, Structure, electronics, and interaction of hydrogen and oxygen on diamond surfaces, *Phys. Rev. B*, 2006, **73**, 085313.
53 M. J. Rutter and J. Robertson, *Ab initio* calculation of electron affinities of diamond surfaces, *Phys. Rev. B*, 1998, **57**, 9241–9245.
54 J. van der Weide, Z. Zhang, P. K. Baumann, M. G. Wensell, J. Bernholc and R. J. Nemanich, Negative-electron-affinity effects on the diamond (100) surface, *Phys. Rev. B*, 1994, **50**, 5803–5806.
55 M. Kataoka, C. Zhu, F. A. M. Koeck and R. J. Nemanich, Thermionic electron emission from nitrogen-doped homoepitaxial diamond, *Diam. Relat. Mater.*, 2010, **19,** 110–113.
56 J. Furthmüller, J. Hafner and G. Kresse, Dimer reconstruction and electronic surface states on clean and hydrogenated diamond (100) surfaces, *Phys. Rev. B*, 1996, **53,** 7334–7351.
57 F. A. M. Koeck and R. J. Nemanich, in *Diamond and Related Materials*, 2005, vol. 14, pp. 2051–2054.
58 M. Suzuki, T. Ono, N. Sakuma and T. Sakai, Low-temperature thermionic emission from nitrogen-doped nanocrystalline diamond films on n-type Si grown by MPCVD, *Diam. Relat. Mater.*, 2009, **18**, 1274–1277.
59 T. Ando, K. Yamamoto, M. Ishii, M. Kamo and Y. Sato, Vapour-phase oxidation of diamond surfaces in O2 studied by diffuse reflectance Fourier-transform infrared and

temperture-programmed desorption spectroscopy, *Journal of the Chemical Society, Faraday Transactions*, 1993, **89**, 3635.
60 J. Ristein, 2004, pp. 37–96.
61 K. P. Loh, X. N. Xie, S. W. Yang and J. C. Zheng, Oxygen adsorption on (111)-oriented diamond: A study with ultraviolet photoelectron spectroscopy, temperature-programmed desorption, and periodic density functional theory, *Journal of Physical Chemistry B*, 2002, 106**,** 5230–5240.
62 K. M. O'Donnell, T. L. Martin, N. A. Fox and D. Cherns, *Ab initio* investigation of lithium on the diamond C(100) surface, *Phys. Rev. B*, 2010, **82,** 115303.
63 P. K. Baumann and R. J. Nemanich, Electron emission from metal-diamond (100), (111) and (110) interfaces, *Diam. Relat. Mater.*, 1998, **7**, 612–619.
64 P. K. Baumann and R. J. Nemanich, Characterization of copper-diamond (100), (111), and (110) interfaces: Electron affinity and Schottky barrier, *Phys. Rev. B*, 1998, **58,** 1643–1654.
65 P. K. Baumann and R. J. Nemanich, Characterization of cobalt-diamond (100) interfaces: electron affinity and Schottky barrier, *Appl. Surf. Sci.*, 1996, **104–105**, 267–273.
66 F. A. M. Köck, J. M. Garguilo, B. Brown and R. J. Nemanich, Enhanced low-temperature thermionic field emission from surface-treated N-doped diamond films, *Diam. Relat. Mater.*, 2002, **11**, 774–779.
67 J. B. Miller, Amines and thiols on diamond surfaces, *Surf. Sci.*, 1999, **439**, 21–33.
68 D. Zhu, J. A. Bandy, S. Li and R. J. Hamers, Amino-terminated diamond surfaces: Photoelectron emission and photocatalytic properties, *Surf. Sci.*, 2016, **650**, 295–301.
69 A. R. Ruslinda, Y. Ishiyama, V. Penmatsa, S. Ibori and H. Kawarada, Repulsive effects of hydrophobic diamond thin films on biomolecule detection, *Appl. Surf. Sci.*, 2015, **328**, 314–318.
70 F. A. M. Köck, J. M. Garguilo, B. Brown and R. J. Nemanich, Enhanced low-temperature thermionic field emission from surface-treated N-doped diamond films, *Diam. Relat. Mater.*, 2002, 11, 774–779.
71 K. Larsson, The Combined Influence of Dopant Species and Surface Termination on the Electronic Properties of Diamond Surfaces, *C (Basel).*, 2020, **6**, 22.
72 K. Kimura, K. Nakajima, S. Yamanaka, M. Hasegawa and H. Okushi, Hydrogen analysis of CVD homoepitaxial diamond films by high-resolution elastic recoil detection, *Nucl. Instrum. Methods Phys. Res. B*, 2002, **190**, 689–692.
73 K. P. Loh, X. N. Xie, S. W. Yang and J. C. Zheng, Oxygen Adsorption on (111)-Oriented Diamond: A Study with Ultraviolet Photoelectron Spectroscopy, Temperature-Programmed Desorption, and Periodic Density Functional Theory, *J. Phys. Chem. B*, 2002, **106**, 5230–5240.
74 P. K. Baumann and R. J. Nemanich, Surface cleaning, electronic states and electron affinity of diamond (100), (111) and (110) surfaces, *Surf. Sci.*, 1998, **409**, 320–335.
75 R. Yoshida, D. Miyata, T. Makino, S. Yamasaki, T. Matsumoto, T. Inokuma and N. Tokuda, Formation of atomically flat hydroxyl-terminated diamond (1 1 1) surfaces via water vapor annealing, *Appl. Surf. Sci.*, 2018, **458**, 222–225.
76 CVD diamond deposition reactors. https://www.chm.bris.ac.uk/pt/diamond/reactors.htm
77 D. N. G. Krishna and J. Philip, Review on surface-characterization applications of X-ray photoelectron spectroscopy (XPS): Recent developments and challenges, *Applied Surface Science Advances*, 2022, **12**, 100332.
78 W. R. Salaneck, Classical ultraviolet photoelectron spectroscopy of polymers, *J. Electron Spectros. Relat. Phenomena*, 2009, **174**, 3–9.

79 J. E. Whitten, Ultraviolet photoelectron spectroscopy: Practical aspects and best practices, *Applied Surface Science Advances*, 2023, **13**, 100384.
80 A. Scholl, in *Reference Module in Materials Science and Materials Engineering*, Elsevier, 2016.
81 M. Al-Kelani and N. Buthelezi, Advancements in medical research: Exploring Fourier Transform Infrared (FTIR) spectroscopy for tissue, cell, and hair sample analysis, *John Wiley and Sons Inc*, 2024, preprint
82 D. Majchrowicz, M. Kosowska, K. Sankaran, P. Struk, M. Wąsowicz, M. Sobaszek, K. Haenen and M. Jędrzejewska-Szczerska, Nitrogen-Doped Diamond Film for Optical Investigation of Hemoglobin Concentration, *Materials*, 2018, **11**, 109.
83 R. Zulkharnay, G. Zulpukarova and P. W. May, Oxygen-terminated diamond: insights into the correlation between surface oxygen configurations and work function values, *Appl. Surf. Sci.*, 2024, **65**8, 159776.
84 M. Müller, M. Schellhorn and K. Mann, Laboratory-scale near-edge X-ray absorption fine structure spectroscopy with a laser-induced plasma source, *J. Anal. At. Spectrom.*, 2019, **34**, 1779–1785.
85 A. Politano, On the fate of high-resolution electron energy loss spectroscopy (HREELS), a versatile probe to detect surface excitations: will the Phoenix rise again?, *Physical Chemistry Chemical Physics*, 2021, **23**, 26061–26069.
86 C. R. Brundle, G. Conti and P. Mack, XPS and angle resolved XPS, in the semiconductor industry: Characterization and metrology control of ultra-thin films, *J. Electron Spectros. Relat. Phenomena*, 2010, **178–179**, 433–448.